DECELERATION DURING IMPACT OF SEAPLANE HULLS ON A WATER SURFACE

by
Bernard d'Utruy
and
A. R. Chamberlain

prepared for the
Department of the Navy
Bureau of Aeronautics
under Contract NOas 55-394-c

in the
Civil Engineering Section
Colorado State University
Fort Collins, Colorado

August 1957

CER58ARC40

DECELERATION DURING IMPACT OF SEAPLANE HULLS ON A WATER SURFACE

by
Bernard d'Utruy
and
A. R. Chamberlain

prepared for the
Department of the Navy
Bureau of Aeronautics
under Contract NOas 55-394-c

in the
Civil Engineering Section
Colorado State University
Fort Collins, Colorado

August 1957

CER58ARC40

TABLE OF CONTENTS

LIST OF FIGURES

LIST OF FIGURES -- Continued

NOMENCLATURE

Symbols	Definition	Dimension
$\acute{a}$	Effective deceleration of hull	L/T^2
α	Dimensionless coefficient	
A	Dimensionless function of angle of dead-rise	L
b	Half width of plate	L
β	Angle of dead-rise	
c	Half wetted width of hull assuming no piled-up water	L
c'	Half wetted width of hull assuming piled-up water	L
η	Dimensionless ratio of immersion depth, z/L	
η_n	Dimensionless ratio of immersion depth at $t = t_n$	
η_m	Dimensionless ratio of immersion depth to maximum deceleration $\ddot{\eta}_m$	
$\frac{d\eta}{d\tau} = \dot{\eta}$	Dimensionless ratio of velocity of hull	
$\frac{d^2\eta}{d\tau^2} = \ddot{\eta}$	Dimensionless ratio of deceleration of hull	
η_n	Dimensionless maximum deceleration	
f, f_1, f_2, f_3	Function relationships	
F	Hull Froude number	
g	Gravitational acceleration	L/T^2
H	Height of drop	L
k	Length parameter	L

NOMENCLATURE -- Continued

Symbols	Definition	Dimension
l	Length of hull	L
L	$=\sqrt{\frac{M}{l}}$ (0.50 ft in these experiments)	L
m	Apparent mass of water	M
M	Mass of hull	M
μ	Coefficient of apparent mass, m/M	
ρ	Mass density of water	M/L^3
ρ_m	Mass density of hull	M/L^3
τ	Dimensionless ratio of time	
τ_m	Dimensionless ratio of time to maximum deceleration $\dot{\eta}_m$	
t	Time	T
V_o	Initial velocity of hull at contact with water surface	L/T
V	Velocity of hull	L/T
V_n	Velocity of hull at $t = t_n$	L/T
Φ	Potential function	L^2/T
Ψ	Stream function	L^2/T
z	Immersion depth below free water surface	L
z_n	Immersion depth below free water surface at $t = t_n$	L
x	Horizontal coordinate of any point	L
y	Vertical coordinate of any point	L

Chapter I

INTRODUCTION

In many problems concerning the impact of a body on a water surface one has to deal with a particular type of flow field which is generated during a fraction of a second. At large impact velocities the field of flow is built up so rapidly that very large forces lead to extremely high stresses in all parts of the body.

Seaplane hulls are designed for minimum deceleration during landing, so as to induce the smallest possible impact forces. Reduced impact loads mean that structural members can be reduced in weight, thus permitting much larger payloads.

For nearly thirty years efforts have been made to derive a means of theoretically and experimentally analyzing the problem of impact of a seaplane hull on a water surface. Two theories have been used nearly exclusively:

(1) the flat plate analogy, and

(2) the expanding prism analogy.

Experiments on the impact of landing are numerous and inconclusive. The ultimate goal during all this research has been to achieve a hull shape that would exhibit uniform deceleration during landing.

This report describes the practical aspects of hydrodynamics of V-wedge hulls and constant-force hulls dropping on a calm water surface.

An experimental determination of the path of particles is compared with the theoretical flow assumed by Wagner (25). The concept of virtual mass of water in the computation of the impact phenomenon is developed and compared with the theory of Von Kármán (24).

Problem

The purpose of this research was to make an experimental study of the impact of V-wedges and constant-force hulls on a calm water surface. The theoretical analysis and experimental research of past investigators will be compared to the experimental results of the present study.

Problem analysis.--The analysis of the problem will consist of the following parts:

1. Investigation of the flow field induced by the impact of wedges, and a comparison of experimental and theoretical particle path lines,
2. Determination of the extent of the flow field,
3. Investigation of the deceleration time-history of the hulls during the impact as a function of time and the angle of dead-rise,
4. Study of the growth of the apparent mass of water associated with the decelerating hull,

5. Comparison of the behavior of the constant-force and V-wedge hulls.

Delimitation of the problem.--In the experiments, V-wedges of 3, 5, 10, 20, 30, 40, and 50 degrees of dead-rise angle and two constant-force hulls of 30 degrees of dead-rise angle were considered. One constant-force hull is the so-called 30 degree constant-force hull and the other is designated X-hull. A detailed description of these hulls is given in Appendices A, B and C. The length of the test hulls is kept at six inches.

Specific delimitations are:

1. All hulls were dropped along the vertical which was normal to the free surface of the water.
2. The hulls were built so that the mass M was the same for all models and equal to 0.1455 slugs for all tests.
3. The height of drop H_o was constant and fixed at five inches. The initial velocity of impact V_o was therefore constant and equal to $\sqrt{2gH_o} = 5.18$ fps. The initial momentum was constant and equal to MV_o. Consequently, the initial conditions for all tests were the same.
4. Since water was used, all fluid parameters were constant during the impact, assuming incompressibility. All the tests were done with water at room temperature, so that the kinematic viscosity was nearly constant.
5. The study was restricted to the two-dimensional case.

Chapter II

REVIEW OF LITERATURE

Although the impact problem has received rather wide attention in the past, until recently most of the studies have been limited to theoretical studies and laboratory measurements of pile-up and deceleration.

The impact problem has been analysed as a potential flow around an immersed body of simple geometrical forms. Most investigators explained the difference between theoretical and experimental results as being due to the effect of spray, the influence of compressibility of fluid and the elasticity of the hull itself.

In presenting the review of literature, the references are not necessarily presented in a chronological order, but in a logical development of the subject.

Von Kármán (24) in 1929 was the first to study the load factor of seaplane hulls. Dealing with the two-dimensional case, his first assumption was the conservation of momentum during the time of impact of the hull on a water surface. He assumed that the momentum of the hull is transferred to a certain mass of water. The apparent mass is the mass of a half-cylinder of water; its diameter is equal to the submerged width $2c$ of the wedge and its length is the length of the hull, l, (see Fig. 1). The mathematical expression of that statement is

$$M\dot{z}_o = (M + m)\dot{z} \,, \tag{1}$$

where

M = mass of the hull

m = apparent mass of water $= \dfrac{1}{\tan^2\beta} \dfrac{\pi\rho}{2} z^2$

H = height of drop

z = displacement of the keel below the water surface

$\dot{z}_o = -\sqrt{2gH}$

$\dot{z} = dz/dt$

ρ = specific mass of water

β = angle of dead-rise.

Wagner (25, 26) considered that since the water displaced by the hull rises along the sides, the width of the wetted surface and the apparent mass are greater than those based upon Von Kármán's theory. In order to evaluate the increased width, Wagner assumed that the particles at the top of the surface move vertically. Utilizing an assumed velocity distribution and integrating for the case of V-wedges, a corrected submerged width $2c'$ is derived,

where

$$\frac{c'}{c} = \frac{\pi}{2} \tag{2}$$

(see Fig. 2).

The assumption that the particles in the wave due to the pile-up move vertically and that the float width at the top of the wave determines the virtual mass seems very arbitrary. This last assumption leads to an apparent mass $(\pi/2)^2$ times that obtained by Von Kármán,

$$m = \frac{\pi^2}{4\tan^2\beta}\,\frac{\pi\rho}{2}\,z^2 \; . \tag{3}$$

Although the method is inadequate, it remains important because a better solution for the case of the float bottom with transverse curvature was not available at the time of the work of Wagner.

Wagner discusses the empirical relation for the apparent mass given by Eq 4,

$$m = \left(\frac{\pi}{2\beta} - 1\right)^2 \frac{\pi\rho}{2}\,z^2 \; , \tag{4}$$

based on constant immersion velocity of the flow about a triangular prism with an angle of dead-rise of 18^0.

<u>Sydow</u> (17) used the latest value of the apparent mass as given by Eq 4 in his investigation. For angles of dead-rise close to 20^0 the result is 1.5 times the apparent mass given by Von Kármán and 0.5 times the apparent mass given by Wagner in his general solution of Eq 3. The importance of the difference is shown by the fact that for equivalent instantaneous conditions these ratios of apparent mass can be regarded as force ratios.

<u>Kreps</u> (6) used the solution of Wagner for the apparent mass. The finite keel factor recommended by Kreps differs from that advanced by Wagner. The aspect ratio factor determined by Pabst (11)

was incorporated in the definition of Kreps of apparent mass of water. Kreps proposed the following formula (Eq 5):

$$m = \frac{\pi^2}{4 \tan^2\beta} (1 - \frac{\beta}{\pi}) \frac{\pi \rho}{2} z^2 . \tag{5}$$

<u>Mayo</u> (7), using Eq 5 and comparing with experimental data showed that a factor 0.82 should be inserted in Eq 4. Therefore, Eq 5 becomes

$$m = 0.82 (\frac{\pi}{2\beta} - 1)^2 \frac{\pi\rho}{2} z^2 . \tag{6}$$

Because of the aspect ratio factor Eq 6 does not hold for small angles of dead-rise. The study indicates that Eq 6 will be satisfactory for angles of dead-rise between 15^0 and 30^0 but begins to be unduly excessive for angles smaller than 10^0. A variation of $\cot^2\beta$ with angle of dead-rise may be better than the variation of $(\frac{\pi}{2\beta} - 1)^2$ with angle of dead-rise.

<u>Monaghan</u> (10) developed a theoretical formula based on the flow about an expanding prism leading to Eq 7,

$$m = \frac{\pi^2}{4}(1 - \frac{\beta}{\pi})^3 \cot^2\beta \ \pi\frac{\rho}{2} z^2 . \tag{7}$$

He also gave a formula for the wetted width computed in the same way as Wagner:

$$c' = \frac{\pi}{2} (1 - \frac{\beta}{\pi}) c . \tag{8}$$

Szebehely (18, 19, 20, 21, 22) derived a mathematical expression for the maximum impact for V-wedge and parabolic wedge. Considering the weight of the float, the momentum equation is

$$1 + \frac{\ell \pi \rho c^2(z)}{2M} \frac{1}{\sqrt{\frac{4c^2(z) + 1}{\ell^2}}} \dot{z} = V_o + gt \quad , \tag{9}$$

and the acceleration is given by Eq 10:

$$- \ddot{z} = \frac{(V_o + gt)\dot{\mu} - g(1 + \mu)}{(1 + \mu)^2} \quad . \tag{10}$$

Further improvement of the determination of the added mass is obtained if the water pile-up is considered. The maximum deceleration $\ddot{z}_m$, if gravity effects are neglected, is computed. It corresponds to the immersion z_m where

$$z_m = \frac{1}{5\alpha'} \quad , \tag{11}$$

with the value

$$-\ddot{z}_m = 1.02 \frac{V_o{}^2}{\beta} \quad , \tag{12}$$

α' being

$$\alpha' = \frac{3}{8Mtg^2\beta} \quad . \tag{13}$$

The time t_m to reach maximum deceleration is

$$t_m = 0.24 \frac{\beta}{V_o} \sqrt{\frac{M}{\rho \ell}} \quad . \tag{14}$$

In fact Eq 12 indicates an infinite impact force for a completely flat bottom. Of course, if the elasticity of the hull plays an important role, the above analysis is invalid.

Szebehely noted that the effect of gravity at the depth z_m of maximum deceleration was very small and therefore can be neglected for small dead-rise angle and large impact velocity.

The suggestion of Crewes mentioned by Ward Brown (27) attempts to systematize aspect ratio correction factors by assuming a linear relation between added mass and the quantity S^2/p, where S is the area and p the wetted perimeter. The justification is that for an elliptic plate the added mass is:

$$m = \frac{8\rho}{3\pi} \frac{S^2}{p} \tag{15}$$

It is interesting to note that the formula of Crewe yields approximately the same results as the finite ratio correction factors obtained experimentally by Pabst (11) and much later by Yu Tach Yu (31).

Ward Brown deals only with the impact of relatively lightly loaded rectangular plane wedges of constant finite dead-rise. He notes that the one possibility that might invalidate the equation of motion is the existence of time lag effects. These effects are analogous to the Wagner effect in aerodynamic theory. As a result of applying steady motion characteristics (slamming) to an unsteady motion (impact), these effects might arise. The Wagner's effect, however, is commonly ignored in aerodynamic theory, and there is as yet no reason to suppose that time lag effects, if they exist, have any significance in hydrodynamic impact theory.

Trilling (23) linearizes the problem of impact and applies classical methods of potential theory to determine the pressure on two-dimensional bodies whose submerged portion may be approximated by a semi-ellipse. Assuming a potential flow, the force is therefore:

$$F = \frac{\rho}{v}\frac{d}{dt}\int \frac{d\varphi}{dn}\, ds \quad . \tag{16}$$

The integration is carried out over the boundaries of the fluid for an elliptic cylinder, of axes 2b and 2a, which strikes the water at an angle θ. The complex flow in the plane ξ is given by Eq 17:

$$F(\xi) = \frac{i\, b \cos\theta}{\pi}\ \frac{1}{\xi} - \xi \ \log\frac{1+\xi}{1-\xi} + i\, a\, \xi \sin\theta \quad . \tag{17}$$

Assuming $a \gg b$, the momentum is given by Eqs 18 and 19:

$$M_x = 2b^2/\pi \tag{18}$$

$$M_y = \pi a^2/2 \tag{19}$$

Bisplinghoff and Doherty (1) summarized in 1950 most of the previous investigations. In general the forces which must be considered when studying the problem of a wedge entering a water surface arise from three sources:

(a) time rate of change of momentum f_u

(b) skin friction drag f_s

(c) buoyancy f_b

The force resulting from (a) is by far the largest of the three and the majority of investigators have neglected (b) and (c) in their studies. Steady state drag coefficients were obtained for wedges with angle of dead-rise β equal to 10^0, 20^0, 30^0, and 40^0 by conducting tests in a water tunnel.

It was shown that in general:

(1) The steady state force f_s was larger than f_b but smaller than f_u.

(2) The expanding prism results are considerably closer to experiments than the results of Wagner. The expanding prism results agree more closely with experiment for $\beta = 20^0$ and 30^0 than for $\beta = 10^0$ and 40^0. A definite trend exists in which the expanding prism results are too high at the low dead-rises and too low at the high dead-rises.

(3) The results of Wagner based on the flow about a flat plate are consistently high.

The ratio c'/c derived by Bisplinghoff and Doherty based on the flow about an expanding prism is high in the low dead-rise range and low in the high dead-rise range.

Bisplinghoff and Doherty studied the case of the two-dimensional impact of seaplane bottoms of arbitrary shapes. Because of the complexity of the problem, two simplifying assumptions were introduced in their theory. They are:

(a) steady-state and buoyancy forces are neglected, and

(b) the instantaneous flow properties are the same as those about a flat plate of width $2c$.

A constant-force hull is derived and agreement between experiment and theory is only fair. The predicted initial value of the impact force is not fully developed and the delicate energy balance required to maintain the constant force is not preserved. As a result the horizontal portions of the bottom near the chines enter the surface at an appreciable velocity and the impact force approaches a second maximum. Failure of the theory to predict the initial value of acceleration may be due to the following:

(a) theoretical assumption of an incompressible fluid, and

(b) lack of understanding of the nature of the water pile-up at low dead-rise angles.

The equation proposed by Milwitzky (9)

$$\frac{c'}{c} = \frac{\pi}{2} \frac{\tan\beta}{\beta} \left(1 - \frac{2\beta}{\pi}\right) , \tag{20}$$

follows the trend of the expanding prism result but is considerably in error at high dead-rise angles.

Schulz (16) made a comparison of the theoretical acceleration history with the actual acceleration history of the constant-force hull. The tests on the theoretically derived constant-force hull for $\beta = 20^0$ indicated that the acceleration did not peak as fast as it was expected. Under the assumption that a hull with an angle of dead-rise less than 10^0 behaved in a similar manner, he deduced that the constant-force hull needed to be flatter over a greater portion of its keel area. He further presumed that the hull should have a slightly steeper angle of dead-rise near the chines; thus the peak in the later part of acceleration history would be avoided. Using a step by step method of empirical corrections a final optimum contour was derived. The hull finally developed by the preceeding procedure had as equivalent angle of dead-rise of 20^0. Hulls where β is equivalent to 30^0 and 40^0 were produced from the dimensionless plot of the hull where β is equivalent to 20^0.

Chapter III

EQUIPMENT AND PROCEDURE

The experimental equipment and the procedure that were employed in utilizing this equipment are discussed under the heading of the specific item of equipment. These are: (1) drop tank, (2) drop mechanism, (3) deceleration measurement device, and (4) flow visualization.

Drop tank

The model hulls were dropped into a rectangular tank made of plexiglass. This tank, which measured six inches wide and three feet high with a four-foot long front wall, was set into a frame of welded angle irons.

At the bottom of the tank a tap was provided to flush out the water after each experiment. Two vertical scales graduated in inches were attached at the front panel to facilitate the measurements taken from photographs. Above the tank, a microswitch, adjustable in height, was mounted on an angle iron and electrically operated the camera shutter as the hull approached the water surface. The tank was set independently from the dropping mechanism.

Drop mechanism

The drop mechanism consisted of a vertical guide for a square rod which moved parallel to it. The model hull was attached to the rod by a 6 x 6 x $\frac{1}{2}$-inch clear plexiglass plate. A hole was provided in the plate of plexiglass for the accelerometer wiring. The rod was made from a piece of $\frac{3}{4}$-inch x $\frac{3}{4}$-inch square brass tubing. The supporting guide was a heavy angle iron with a lock to immobilize the rod supporting the hull before dropping.

Hulls

V-wedge hulls of 10, 20, 30, 40 and 50 degrees of angle of dead-rise, and the constant-force hull were the same as used by E. F. Schulz in 1954. The three- and five-degree hulls and the X-hull were built in the Colorado State University Hydraulics Laboratory by the same method as that used by Schulz (16).

All models were constructed of mahogany, the surfaces of which were sanded and painted with six coats of Periseal. The inside of the hulls were hollowed out to receive the accelerometer. Metal ballast was added as necessary to maintain the constant mass M of the hull (0.1455 slugs). All hulls were six inches long. The geometrical dimensions of the V-wedges are given in Appendix A. Figure 4 shows the general cross-section of a hull provided with accelerometer and rod.

The dimensions of the X-hull were graphically obtained by reading the x^* and y^* coordinates of a seaplane forebody at an arbitrary section. The beam was 11 inches and the angle of dead-rise 31^0 $10'$. This template was reduced to a beam of 9.5 inches and to an angle of dead-rise of 30^0.

The X and Y coordinates are given by Eqs 21 and 22:

$$X = 9.5/11 \ x^* = 0.864x^* \tag{21}$$

$$Y = \frac{9.5}{11} \frac{\tan 30^0}{\tan 31^0 10'} y^* = 0.825y^* \tag{22}$$

The results are shown in Appendix B.

<u>Deceleration measurement device</u>

<u>Accelerometer</u> -- The deceleration time history was obtained by means of a Statham Model A8-10-335 accelerometer. The accelerometer was bolted to the inside of the hull (Fig. 4). The shielded flexible accelerometer lead passed through the hull cover plate and was formed in a loop to permit free motion of the hull. The accelerometer had a natural frequency of 250 cps and was able to record acceleration between $\pm$ 10g. The signal from the accelerometer was transmitted to the screen of an oscilloscope. A camera recorded the image which appeared on the oscilloscope screen.

<u>Oscilloscope</u> -- The arrangement was the same as that used by Schulz (16). The oscilloscope was a Model 304 A Dumont, which was equipped with a special short-persistance blue cathode ray tube and a driven sweep. This oscilloscope was specially designed for photographing these relatively low frequency transient signals.

<u>Oscilloscope camera</u> -- The camera was a Fairchild oscilloscope camera, which was equipped with an f2.8 Wollensak

coated lens mounted in a Rapax shutter and equipped with a Polaroid-land back. A print of the record can be obtained within a few minutes after exposure. The shutter of the camera was set at "B" and operated from the microswitch mentioned earlier.

Flow visualization

Birefringent solution method -- The property of doubly-refracting bentonite suspensions was used to make the flow pattern visible during the water-hull impact. A small tank, one foot deep, three inches thick and two feet long, was built to test the possibility of using this technique. A solution of three percent of Californian bentonite was adopted to produce sufficient birefringence in order to get any significant amount of information. However, the experiment ran into difficulties with thixotrophy. To eliminate flocculation, sodium carbonate was added to the solution; only slight deflocculation was noted.

Beside these handicaps, it was noted that the maximum deceleration of the hulls occurred within the first 0.01 of a second. Experiments indicated that the reaction time interferred with the phenomena of flow visualization. Under a six-inch depth of fluid, the polarized light was completely diffused.

Neutral buoyancy bubble method -- It was required to have a solution which was transparent and insoluble in water, and whose density was the density of the water in the test tank during the experiment. This solution was made with carbon tetrachloride (unit weight = 1.59 g/ml) and xylene (unit weight = 0.86 g/ml). These were mixed in the approximate ratio of one part to three parts by volume. The mass density of the bubble solution was adjusted before each experiment by a trial and error method.

By means of a syringe with a small brass tube tapered at one end, spherical droplets of about $\frac{1}{8}$-inch in diameter were placed approximately in the main central plane of flow.

The tank was illuminated from the back by a one-hundred-watt photoflood reflector. The spherical droplets of the solution, having a different index of refraction from the water, acted like a convergent lens of very small focal distance and produced a refracted beam of wide dispersion. To obtain an intense brightness of the droplets, the reflector was set one foot from the tank and illuminated one-half of the flow field. The beam from the reflector was directed at approximately 45 degrees to the plane of flow in the tank. The camera was placed three feet away from the tank normal to the plane of flow but out of the glaring light of the reflector (See Fig. 5). With such a device, the contrast was satisfactory, and each droplet looked like a bright star in a dark sky.

A 4 x 5-inch Speed Graphic camera with an f2.8 lens was used for obtaining the photographs of the path of the droplets during the impact. The aperture was set at f5.6 and Tri-X film was used. The camera, fixed at a speed of $\frac{1}{25}$ of a second, was triggered by an adjustable microswitch. The switch, mounted on the tank, was activated by a cam fixed on the rod (Fig. 4). By adjusting the position of the switch on the tank, the time of photographing, relative to the initial impact, could easily be adjusted. For each hull, a series of photographs showing the progressive evolution of the flow field was thus obtained.

Chapter IV

THEORETICAL ANALYSIS

This chapter presents a theoretical analysis of the impact problem. It can be divided into three main parts: (a) momentum equation; (b) study of the deceleration, and (c) determination of the flow field.

Momentum equation

An expression for the apparent mass of water set into motion when a hull strikes a calm water surface can be developed from consideration of the conservation of momentum.

Consider a wedge (see Fig. 1) of mass M angle of deadrise β and density ρ_m. Let the velocity of the wedge when it hits the water be V_o. As it moves downward from the water surface, more and more water is brought into motion. From the principle of conservation of momentum, the momentum of the wedge at a distance below the water surface, plus the momentum of an apparent mass of water m having the same velocity dz/dt as the wedge, would remain constant and equal to the initial momentum of the wedge. That is,

$$MV_o = (M + m)\ dz/dt \quad , \tag{23}$$

or

$$V_o = (1 + \mu)\ dz/dt \quad , \tag{24}$$

in which $\mu = m/M$ is the coefficient of apparent mass of water. It is obvious from physical reasoning that m is a function of the immersed depth z and the angle of dead-rise β times the specific mass of water ρ and the length of hull ℓ. Thus m can be expressed as

$$m = \rho f(z, \beta) \ell , \tag{25}$$

or

$$\frac{m}{M} = \frac{\rho f(z, \beta) \ell}{\rho_m L^2 \ell} , \tag{26}$$

where

$$M = \rho_m L^2 \ell , \tag{27}$$

in which L is defined by

$$L = \sqrt{\frac{\text{Mass of hull}}{\rho_m \ell}} . \tag{28}$$

Eq 26 can be reduced to

$$\mu = \frac{m}{M} = \frac{\rho}{\rho_m} \frac{f(z, \beta)}{L^2} . \tag{29}$$

Under the assumption that f is a product of $f_1(\beta)$ and $f_2(z^n)$ Eq 29 becomes

$$\mu = A(\beta) \frac{f_2(z^n)}{L^2} , \tag{30}$$

where $A(\beta) = \frac{\rho}{\rho_m} f_1(\beta)$.

Since Eq 30 is a physical equation, and μ nondimensional, $f_2(z^n)$ is a homogeneous function. Thus Eq 30 can be written in the form

$$\mu = A\, f_3(z^n/L^2) \quad , \tag{31}$$

where f_3 must also be dimensionless, since A is nondimensional. This is possible if $n = 2$ or if f_3 is of the form f_3 is of the form $f_3[(z/L)^2 + \alpha]$. Experimental work done by the previous investigators show that $n = 2$ does not give good results. Therefore, let

$$\mu = A\, f_3[(z/L)^2 + \alpha] \quad . \tag{32}$$

If f_3 is taken as the simple form

$$f_3\,[(z/L)^2 + \alpha] = (z/L)^2 + \alpha \quad , \tag{33}$$

the momentum Eq 24 now can be written as

$$V_o = [1 + A\,(z/L)^2 + \alpha] dz/dt \quad . \tag{34}$$

Equation 34 can be made dimensionless with the dimensionless variables $\eta = z/L$ and $\tau = tg/V_o$. Therefore,

$$F^2 = [1 + A\,\eta^2 + \alpha]\,\frac{d\eta}{d\tau} \quad , \qquad [35]$$

in which $F = V_o/\sqrt{gL}$ can be called a wedge Froude number.

<u>Study of the deceleration</u>

Solving Eq 35 for $d\eta/d\tau$, it becomes

$$\frac{d\eta}{d\tau} = \frac{F^2}{1 + A\eta^2 + \alpha} \quad , \qquad [36]$$

The deceleration $\frac{d^2\eta}{d\tau^2} = \ddot{\eta}$ is obtained by differentiating Eq 36 with respect to time and can therefore be expressed as a function of

$$\ddot{\eta} = -F^2 \frac{A(2+\alpha)\,\eta^{1+\alpha}}{(1 + A\eta^{2+\alpha})^2}\ \dot{\eta} \quad , \tag{37}$$

or

$$\ddot{\eta} = -F^4 A(2+\alpha) \frac{\eta^{1+\alpha}}{(1 + A\,\eta^{2+\alpha})^3} \quad . \tag{38}$$

Since $\ddot{\eta}$ is a continuous function for positive values of and has the value zero when $\eta = 0$, and zero again when $\eta \rightarrow \infty$, the deceleration has a maximum. The maximum deceleration $\ddot{\eta}_m$ is reached when the derivative $d\,\ddot{\eta}/d\eta = 0$; i.e., when

$$F^4 A\,(2+\alpha)^{\alpha}_{\eta} \frac{A(5+2\alpha)\,\eta^{2+\alpha} - (1+\alpha)}{(1 + A\,\eta^{2+\alpha})^4} = 0 \quad . \tag{39}$$

this occurs when

$$\eta \equiv \eta_m = \frac{1+\alpha}{A(5+2\alpha)}^{\frac{1}{2+\alpha}} \quad . \tag{40}$$

Substituting the value of η_m given by Eq 40 into Eq 38, the maximum deceleration is

$$\ddot{\eta}_m = -F^4 A \frac{(5+2\alpha)^3}{27(2+\alpha)^2} \left[\frac{1+\alpha}{A(5+2\alpha)} \right]^{\frac{1+\alpha}{2+\alpha}} . \tag{41}$$

Integration of Eq 34 yields the dimensionless variable τ as a function of the dimensionless variable η, or

$$\tau = \frac{1}{F^2} \left[\eta + \frac{A}{3+\alpha} \eta^{3+\alpha} \right] . \tag{42}$$

The value of τ_m for which the deceleration is maximum is obtained by substituting the value of η_m given by Eq 40 into Eq 42

$$\tau_m = \frac{\eta_m}{F^2}\left(1 + \frac{A}{3+\alpha}\eta_m^{2+\alpha}\right) \qquad (43)$$

<u>Determination of the flow field</u>

The problem to be considered is the determination of the properties of the two-dimensional unsteady flow pattern in the vicinity of a wedge entering the surface of a fluid.

It is assumed that the hull is of infinite extent, that the fluids extend to infinity along and below its surface, that a potential flow exists, that the flow pattern is the same as if the hull were immersed in the fluid and represented by the flow around a plate in translation normal to the plate. If the width of the plate is 2b and its velocity V, the complex flow given by Bisplinghoff (1) for the steady case in the Argand plane z is

$$\Phi_s + i\Psi_s = -iV\sqrt{z^2 - b^2}\,. \qquad (44)$$

Separating the imaginary and real parts of Eq 44, the equation of the stream lines for the steady case is

$$\Psi_s = \pm V\sqrt{\frac{(x^2 - y^2 - b^2) \pm \sqrt{(x^2 - y^2 - b^2)^2 - 4x^2y^2}}{2}} \qquad (45)$$

The stream function for a uniform flow of velocity V is

$$\Psi = Vx \tag{46}$$

The stream function Ψ_u for the unsteady case is the sum of the two stream functions Ψ' and Ψ_s given by Eqs 45 and 46

$$\Psi_u = \Psi_s + Vx = kV = \text{Constant} . \tag{47}$$

Where kV is the streamline parameter and k a length parameter. The solution of Eq 47 for y^2 yields

$$y^2 = (x - k)^2 \left[\frac{b^2}{k(2x - k)} - 1 \right] . \tag{48}$$

The streamlines are shown on Fig. 23.

Chapter V

PRESENTATION OF DATA

Presentation of data is presented under four main headings: (1) numerical method of computation, (2) determination of coefficient of apparent mass for V-wedges, (3) constant-force hulls, and (4) flow field extension.

Numerical method of computation

In analyzing the results of the experiments given by the time-history curves, it was necessary to compute the velocity V and the immersion depth η of hulls at the time t. The method of computing each of these quantities is presented below and the results are presented in Appendix D.

Velocity -- The velocity V_n was obtained by a numerical integration of the deceleration-time history curves given by the oscilloscope. At the very beginning of the impact, the acceleration a is $+g$. Consequently, the value of the deceleration was measured in the positive direction on Fig. 3 from $a = +g$. At the time t_n the velocity V_n is given by

$$V_n = V_o - \int_o^{tn} a \, dt \quad . \tag{49}$$

The trapezoidal rule for evaluating this integral is

$$V_n = V_o - \sum_1^n g \frac{a_{n-1} + a_n}{2} \Delta t \tag{50}$$

Δt being equal to 0.001634 sec. and V_o equal to 5.18 fps. Eq 51 gives the value of the velocity V_n in fps when $t = t_n$. Therefore,

$$V_n = 5.18 - 0.0525 \sum_1^n \frac{a_{n-1} + a_n}{2} \quad . \tag{51}$$

Immersion depth -- The immersion depth η_n is obtained by integration of the velocity function with respect to time. At the time t_n the depth η_n is

$$\eta_n = \frac{1}{L} \int_o^{t_n} V dt \tag{52}$$

η_n being computed by the same procedure as is used for the velocity with $\Delta t = 0.001634$. Therefore,

$$\eta_n = 0.00345 \sum_1^n \frac{V_{n-1} + V_n}{2} \quad . \tag{53}$$

Coefficient of apparent mass -- The coefficient of apparent mass μ_n is given by Eq 24. Therefore,

$$\mu_n = V_o / V_n - 1 \quad . \tag{54}$$

Determination of the coefficient of apparent mass

According to Eqs 32 and 33, μ is determined by knowing the two functions α and A.

Determination of α -- Consider the log-log plot of μ versus η (Fig. 7). The density of the hull being less than the density of water, one can expect a maximum immersion depth at which V_n tends to zero and μ tends to infinity. Consequently, all curves have to be asymptotic to a certain straight line η = constant. Under these conditions for a practical problem, one can neglect the curved portion of the graph for which μ is greater than unity. The remaining portion $(0<\mu<1)$ can be approximated by a series of straight lines. It is significant that the slope of the straight lines $2+\alpha$ is constant. This indicates that α, which has the value 0.15, is independent of the angle of dead-rise β. In drawing these lines, there was a variation in α of approximately five percent. The coefficient of apparent mass can be written as

$$\mu = A(\beta)\,\eta^{2.15} \quad . \tag{55}$$

Determination of A -- The parameter A in Eq 55 can be evaluated in the following way. When $\mu = 1$, one obtains

$$\eta_{\mu=1} = A^{-1/2.15} \quad . \tag{56}$$

The variation of $\eta_{\mu=1}$ with β (Fig. 8) can be represented by the equation

$$\eta_{\mu = 1} = \text{Const.} \ (\beta + \beta_o)^{1.75} \ ,$$

where $\beta_o = 12^0$. Therefore, $\eta_{\mu = 1}$ can be obtained directly for a given value of β. Substituting this value in Eq 55, A can be evaluated. Thus A will be given by

$$A = \frac{9.3 \times 10^6}{(\beta + 12)^{3.76}} \ . \qquad (57)$$

The substitution of Eq 57 in Eq 55 gives

$$\mu = \frac{9.3 \times 10^6}{(\beta + 12)^{3.76}} \eta^{2.15} \ . \qquad (58)$$

The introduction of the angle $\beta_o = 12^0$ for all V-wedge hulls bound the value of μ when β tends to zero. Most investigators have obtained for A a function depending on β such that A tends to infinity when β tends to zero. It is felt that Eq 58 can be used for values of β smaller than three degrees and results for the flat plate may be obtained. The angle β_o is a correction angle due to the fact that at the beginning of the impact, which occurs in a very short time, a very restricted part of water is set into motion with a lag of time. The latter is caused particularly by the elasticity of hull and water. Hence, β_o is then assumed to be a function of the celerity of an elastic wave.

Maximum deceleration for V-wedges

The theory is compared with the experimental results on (1) the maximum deceleration η_m, (2) the immersion depth η_m, (3) the value of τ_m to maximum deceleration.

Maximum deceleration -- The substitution of μ given by Eq 58 in the theoretical Eq 41 gives the following expression for the maximum deceleration $\ddot{\eta}_m$

$$\ddot{\eta}_m = \frac{2.80 \times 10^3}{(\beta + 12)^{1.75}} \quad . \tag{59}$$

Figure 9 shows the plot of Eq 59 versus β with the experimental results of Bisplinghoff (1) and the results of the present investigation. The results of the present investigation are in agreement to an approximation of less than five percent for all V-wedges except the 30^0 hull. For the latter case the result is within eight percent of the curve, Bisplinghoff's results are higher than theoretical results and also higher than the results of the present investigation. This discrepancy can be explained by the consideration that the drop tank of Bisplinghoff was smaller than the tank used in this study. The proximity of the boundary would increase the resistance to the expansion of the flow during the impact and consequently would increase the value of the maximum deceleration.

Immersion depth η_m to maximum deceleration -- Substituting the value of A and α in the theoretical Eq 40 one gets the following expression for the immersion depth η_m to maximum deceleration,

$$\eta_m = 2.85 \times 10^{-4} \ (\beta + 12)^{1.75} \quad . \tag{60}$$

Figure 10 shows the plot of η_m versus β on which are plotted the experimental results of the present investigation as well as the results of Bisplinghoff. One can see that experimental results for 3, 5, and 30 degree hulls are within reasonable agreement with the theoretical result; for the 10, 20, and 40 degree hulls the approximation reduces to ten percent. Equation 60 shows that when β tends to zero, τ_m tends to 0.015.

Value of τ_m to maximum deceleration -- The expression for the time to maximum deceleration as a function of the angle of deadrise is obtained by substitution of A and α in Eq 43. Hence, one gets

$$\tau_m = 1.74 \times 10^{-4} (\beta + 12)^{1.75} . \qquad (61)$$

Figure 11 shows the plot of τ_m versus β. The experimental results for the 3, 10 and 30 degree hulls agree very well with the theory; agreement reduces to 12 percent for the 5 degree hull and 30 percent for the 40 degree hull. For the latter case, the lack of accuracy may be due to the fact that the deceleration-time history curve given by the oscilloscope has an origin which is difficult to determine experimentally. In that case, the beginning of the impact can only be determined within 0.02 second accuracy. In the case of the 50 degree hull this error was of very large magnitude. For this reason, even though some data were taken for this hull, they are not presented.

Constant-force hulls

Figure 12 shows the plot of the deceleration versus time for the constant-force hull. One can see two maxima for the 30 degree constant-force hull and for the X-hull. It should be noted that the profile of both hulls have two flat portions - at the chine and the keel - separated by an inflexion point. The "drop" of those hulls can be a composite effect of two consecutive hypothetical V-wedges.

Consequently, the two flattest parts of the profile will produce two maxima accelerations. For the X-hull, the first maximum deceleration reaches -1.6 gravities whereas for the 30 degree constant-force hull the first maximum deceleration reached -2.2 gravities. An opposite trend occurs for the second maximum deceleration. The second maximum deceleration are respectively -2.6 and -1.6 gravities.

For both hulls, the time separating the two maxima is equal to 0.03 seconds.

A log-log plot of the coefficient of apparent mass μ versus the immersion depth η is represented in Fig. 13. One cannot differentiate the 30 degree constant-force hull and the X-hull from each other, but one can still represent μ by the form

$$\mu = A\,\eta^{2+\alpha} \tag{62}$$

Assuming that $\beta_o = 12$ remains the same for the two different types of hulls, A would have the same value as a V-wedge of 22 degrees angle of dead-rise. It is important to note that in this case α is negative and is equal to 0.15. On the other hand, in the case of a V-wedge α had a positive value. Under these considerations Eq 34 becomes

$$\mu = A\,\eta^{1.85} \tag{63}$$

whereas for V-wedges $\mu = A\,\eta^{2.15}$.

One can conclude that, for a given value of η , the coefficient of apparent mass μ for constant-force hulls (μ less than one) is larger than that corresponding to a 30 degree V-wedge hull. The maximum deceleration for constant-force hulls is, therefore, expected to be less than the maximum deceleration of the latter.

Flow field extension

According to Eq 48, a series of flow fields corresponding to different plate lengths 2b were drawn and compared with the experimental flow field obtained from the photograph. The photographs were taken at a speed of 0.04 seconds, whereas the duration of the flow phenomenon is less than that. A study of the variation of hypothetical plate lengths with different variables, therefore, is very difficult. The stream function given by the flow around an immersed plate with uniform translation in the direction normal to the plate can be represented by the experimental stream lines around the wedge obtained from the photograph. For an angle of dead-rise greater than five degrees the hypothetical length 2b of the flat plate was observed to increase with the immersed depth; below 10 degrees, the length 2b was observed to be independent of immersed depth.

It was further observed that the computed stream lines did not agree with the experimental stream lines very near the hull (about an inch from the hull), if the angle of dead-rise was greater than 30^0 .

The ratio c/b (corresponding to Wagner's $c'/c = 1.6$) was found to be less than Wagner's value. For a small angle of dead-rise c'/b had the value 1.2. However, this value increases slightly with increase of the angle of dead-rise.

For all hulls the spray root of water due to the impact followed a definite plane which is slightly less than $\beta/2$ as shown in the picture by a bright line.

It was also observed that an easily measurable effect of impact in the developing flow field is limited to a distance of approximately one foot from the hull although there was a flow at greater distances.

Flow fields at several immersion depths during impact and theoretical stream lines are shown in Figs. 14 through 23.

Chapter VI

CONCLUSIONS

Analysis of data for the impact of wedges has yielded information on the associated apparent mass of water. One can conclude that:

1. The apparent mass of water is not proportional to the second power of immersion depth, but to a power higher than two for V-wedge hulls and less than two for constant-force hulls.
2. The introduction of the coefficient β_0 in the expression of the apparent mass of water can probably be considered as mainly due to the elasticity of hull and water. As a result, the value of maximum deceleration for small angle of dead-rise is bounded.
3. The tests on the constant-force hulls indicate that the maximum deceleration can be reduced from two g's for the 30 degree V-wedge to 1.8 g's for the two 30 degree constant-force hull. The presence of two peaks in the deceleration curves for the constant-force hulls can only be explained on the basis of physical reasoning.
4. The extent to which the flow field expanded in the present series of tests indicates that it is probably

necessary to consider the effect of boundary proximity on the flow field for small tank experiments.

5. Flow visualization by means of a birefringent dilute suspension of bentonite was not possible with available equipment. Diffusion of light by the six inch thick bentonite and water suspension was too great to enable one to obtain useful results in the drop tank employed.

6. Neutral buoyancy bubbles immersed in water, in conjunction with a light source, was a suitable flow visualization technique. This method made it possible to obtain photographic records of the flow field generated by the dropping hulls. The time exposure necessary for obtaining satisfactory photographs was a problem. The neutral buoyancy bubble technique, while satisfactory, needs some further refinements.

The momentum equation seems to be satisfactory for studying problems of impact. However, some suggestions can be made for further investigations:

1. There is a need to investigate further the effect of the properties of the hull material on the problem of impact.

2. More information about the impact of a flat plate would be useful.

BIBLIOGRAPHY

1. Bisplinghoff, R. L. and Doherty, C. S. A two dimensional study of the impact of wedges on a water surface. Cambridge, Massachussetts, Massachussetts Institute of Technology. Department of Aeronautical Engineering, March 1950. 115p.
   (Contract No. NOa(s)-9921 for Bureau of Aeronautics.)

2. Benscoter, S. U. Effect of partial wing lift in seaplane landing impact. U. S. National Advisory Committee for Aeronautics. Technical note No. 1563:1-14, April 1948.

3. Cooper, E. P. Theory of water entry of missiles with flat noses. Underwater Ballistics Conference. Proceedings, 8:Part I:15-16, 1950.

4. Hobbs, E. V. Experimental determination of virtual mass from measurement of forces developed during entry of a sphere into water. U. S. National Bureau of Standards Laboratory. No. 6.4/196 PR 4. NAonr 8-48 Amend 1, 1780317, Res. Navy, 1948, September 1950.
   (Cited in Hobbs, Breakstone and Woodson (5).)

5. Hobbs, E. V. and Breakstone, H. I. and Woodson, J. B. Oblique entry of spheres into water. U. S. National Bureau of Standards. Report 2788:1-26, August 16, 1954.

6. Kreps, R. L. Experimental investigation of impact in landing on water. U. S. National Advisory Committee for Aeronautics. Technical memorandum, No. 1046:1-35, 1943.

7. Mayo, W. L. Analysis and modification of theory for impact of seaplanes on water. U. S. National Advisory Committee for Aeronautics. Technical note No. 1008:1-34, 1945.

8. McPherson, A. E., Byers, H. L. and Hobbs, E. V. Experimental determination of virtual water mass from measurement of forces developed during entry of prismatic solids into water. U. S. National Bureau of Standards Laboratory. Report No. 6.4/1-196, PR 2. NAonr 8-48 Amend 1, 1780317, Res. Navy, 1948, December 1949.
   (Cited in Hobbs, Breakstone and Woodson (5).)

9. Milwitzky, Benjamin. A generalized theoretical and experimental investigation of the motion and hydrodynamic loads experienced by V-bottom seaplanes during stoplanding impacts. U. S. National Advisory Committee for Aeronautics. Technical note, No. 15161-60, February 1948.

10. Monaghan, R. J. and Crewe, P. R. Formulae for estimating the forces in seaplane-water impacts without rotation or chine immersion. RAE Rep. Aero. 2308. January 1949.
Summarized in Ward Brown, P. Seaplane impact theory. Short Brothers and Harland, Ltd. Hydrodynamics note No. 46:1-14, August 1954.

11. Pabst, Wilhelm. Theory of landing impact of seaplanes. U. S. National Advisory Committee for Aeronautics. Technical memorandum No. 624:1-29, June 31, 1931.
(Translation from Zeitschrift fur Flugtechrich und Motorluftschiftabrt, January IV, 1931, Vol. 21, No. 1.)

12. Richardson, E. G. The impact of a solid on a liquid surface. Physics Society, Proceeding 61:352-367, October 1948.

13. Robertson, B. C. The development of a flow visualization technique. National Gas Turbine Establishment, Pyestock, Hands. Report, No. R 181:4-23, November 1955.

14. Rosemberg, Benjamin. The use of doubly refracting solutions in the investigation of fluid flow phenomena. U. S. Navy Department. The David W. Taylor Model Basin Report, 617:1-39, March 1952.

15. Schiffman, M. and Spencer, D. C. The force of impact on a sphere striking a water surface. New York, New York University, Applied Mathematics Group, February 1945. 47 p.
(Allied Mathematics Plane Report 42.1R; - AMG-NYU No. 105.)

16. Schulz, E. F. Development of a constant-force bottom contour seaplane hulls. Fort Collins, Department of Civil Engineering, Colorado Agricultural and Mechanical College, 1954, 41p. (Report No. 54EFS31).

17. Sydow, J. Uber den Eiufluss von Tederung und Vielung aub den Laudestoss. Detche Luftfahrtforschung Jahrbuch, Vol. 1:329-338, 1938.

18. Szebehely, V. G. Hydrodynamic approach to the slamming of ships. Midwestern Conference on Fluid Mechanics. Proceedings, 2:89-97, 1952.
(Ohio State University Engineering Experiment Station. Bulletin 149).

19. Szebehely, V. G. Hydrodynamics of slamming of ships. U. S. Navy Department. The David W. Taylor Model Basin. Report, 823:1-31, July 1952.

20. Szebehely, V. G. On slamming. U. S. Navy Department. The David W. Taylor Model Basin. Report, 995:1-42, January 1954.

21. Szebehely, V. G. and Brooks, S. H. Preliminary experimental investigation of slamming. U. S. Navy Department. The David W. Taylor Model Basin. Report, 812:1-12, July 1952.

22. Szebehely, V. G. and Zarnick, E. E. Hydrodynamic impact measurement. U. S. Navy Department. The David W. Taylor Model Basin, 1955, 26p.
(First Conference on Coastal Engineering Instrument, 1955.)

23. Trilling, Leon. The impact of a body on a water surface at an arbitrary angle. Journal of Applied Physics, 26:161-170, February 1950.

24. Von Karman, Th. The impact of seaplane floats during landing. U. S. National Advisory Committee for Aeronautics. Technical note No. 321:1-8, 1929.

25. Wagner, H. Landing of seaplanes. U. S. National Advisory Committee for Aeronautics. Technical memorandum No. 622:1-15, 1931.

26. Wagner, H. Impact forces at water entry. Underwater Ballistics Conference Proceedings 8:Part I:3-13, 1950.

27. Ward Brown, P. An empirical analysis of the planning characteristics of rectangular flat-rates and wedges. Short Brothers and Harland Ltd. Hydrodynamics note, No. 47:1-31, September 1954.

28. Watanabe, S. Resistance of impact on water surface. Tokyo Institute of Physical and Chemical Research. Scientific Papers 226:251-266, 1930.

29. Wendel, Kurt. Hydrodynamic masses and hydrodynamic moments of inertia; translated by E. N. Labouvie and Avis Borden. U. S. Navy Department. The David W. Taylor Model Basin. Translation 260:1-81, July 1956.
(Translation of Wendell Kurt. Hydrodynamische Massen und Hydrodynamishe Massentragheitsmomente. Jahrb. d. STG, Vol. 44, 1950.

30. Weible, A. The penetration resistance of bodies with various head forms at perpendicular impact water. U. S. Office of Naval Research. Naval Research Laboratory. Translation, No. 286:1-30, February 1952.
(German aviation research report No. 4551) Translation of Weible, A. Der Eindringswiderstand von Korpern mit vershiedenen Kopffermen bei senkrechtem Aufschlag auf Wasser.

31. Yu, Yee-Tak. Virtual masses of rectangular plates and parallelepipeds in water. Journal of Applied Physics, 16:724-729, November 1945.

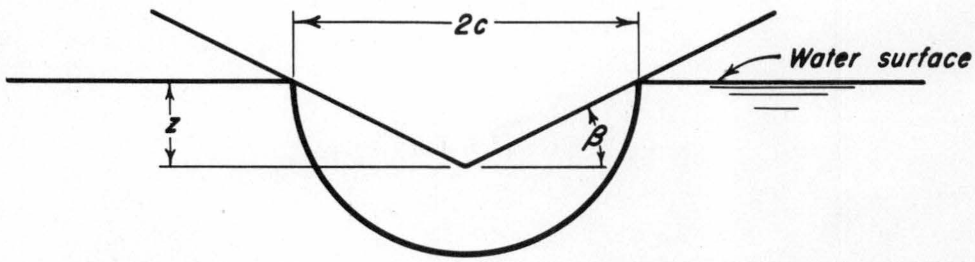

Fig. 1 Diagram of apparent mass for two-dimensional hull as given by von Kármán

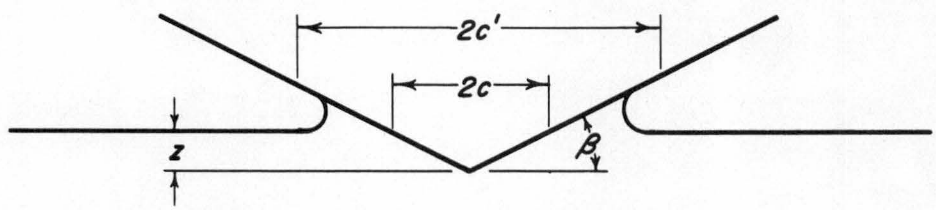

Fig. 2 Definition sketch for water pile-up on a V-wedge hull as given by Wagner

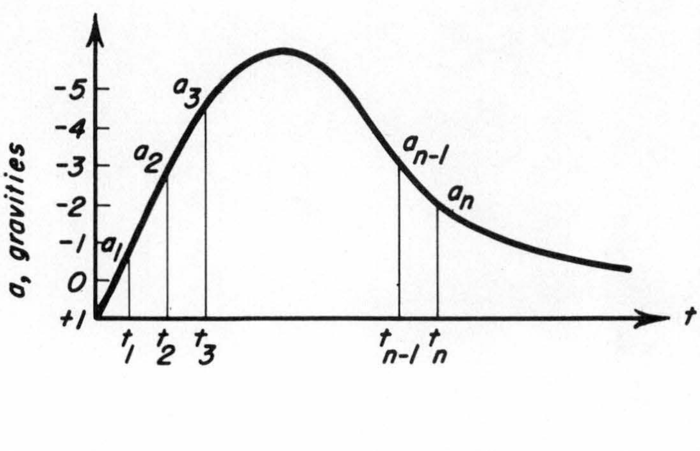

Fig. 3 Typical effective deceleration — time history

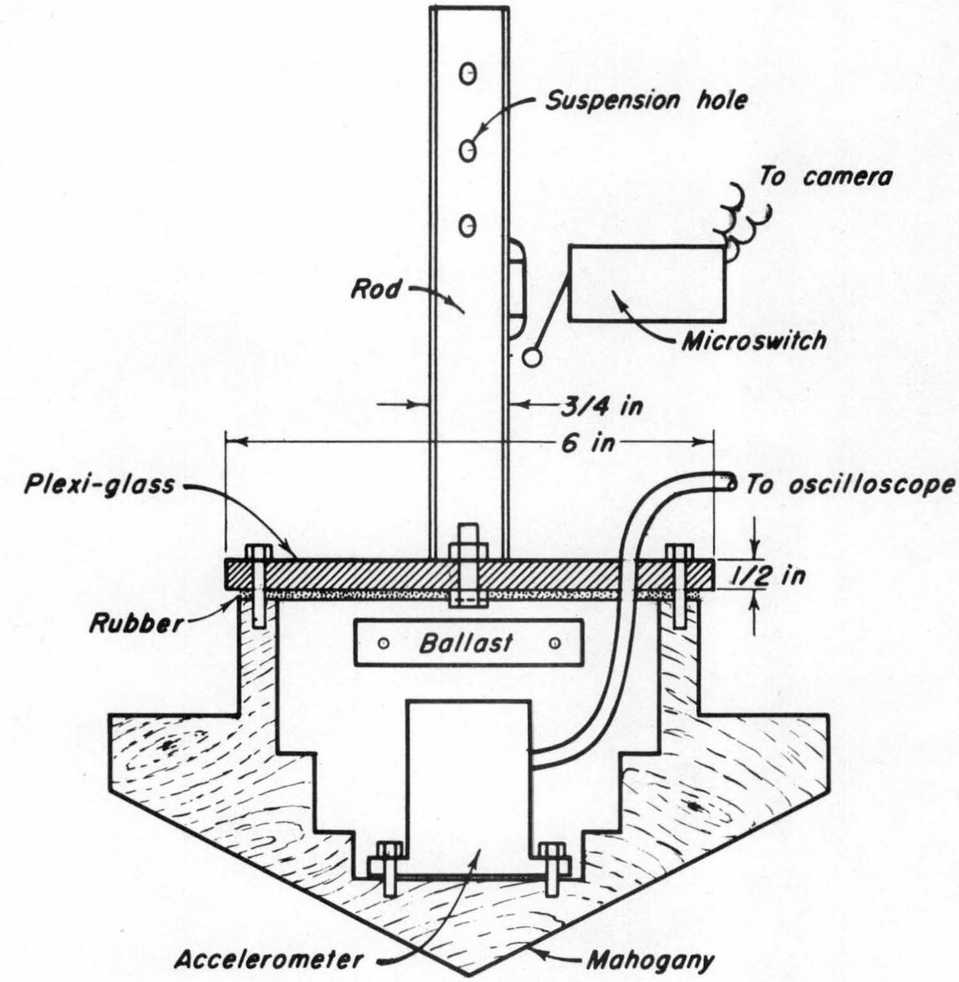

Fig. 4 Cross-section of hull

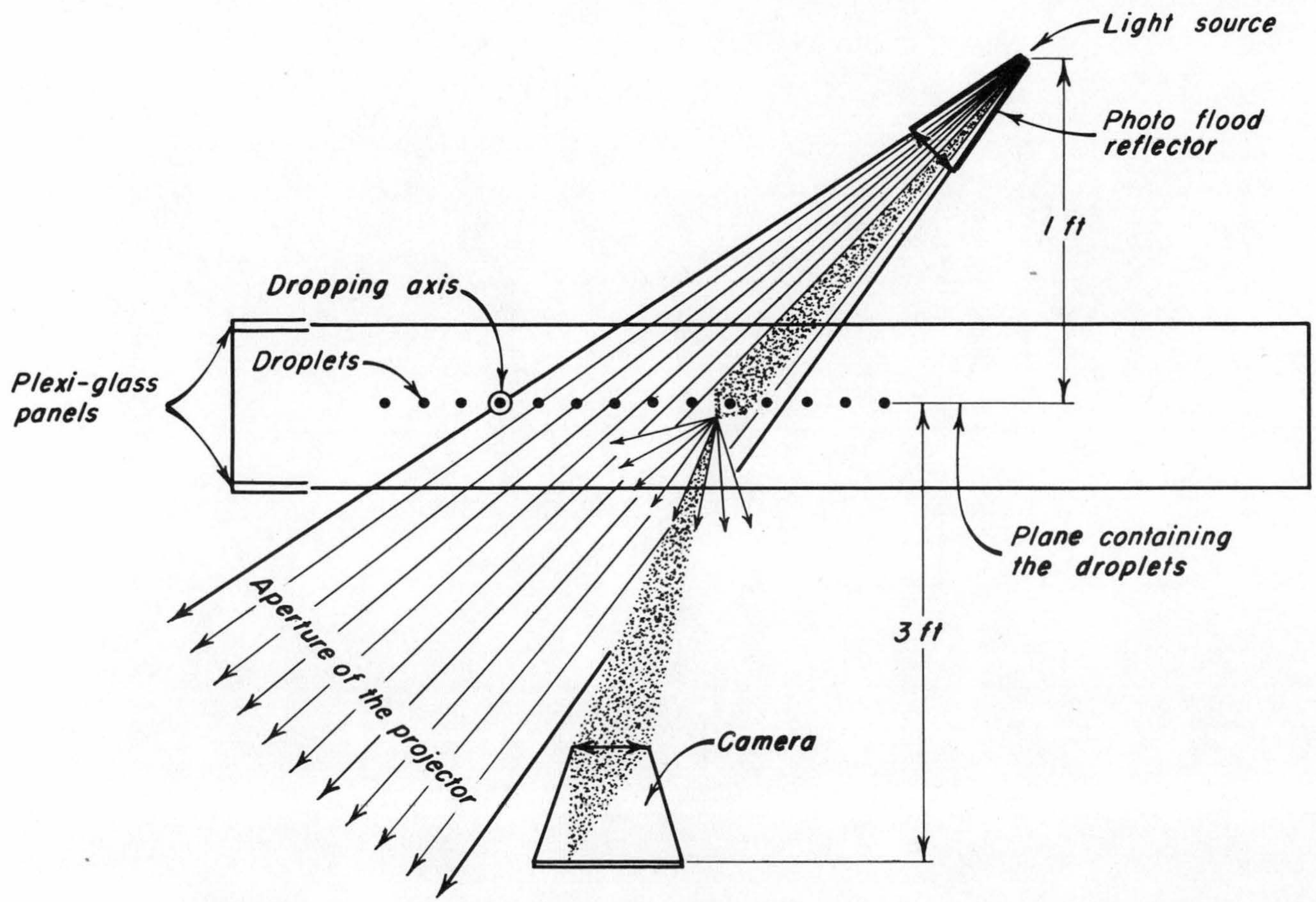

PLAN

Fig. 5 Schematic diagram of illumination device for flow visualization

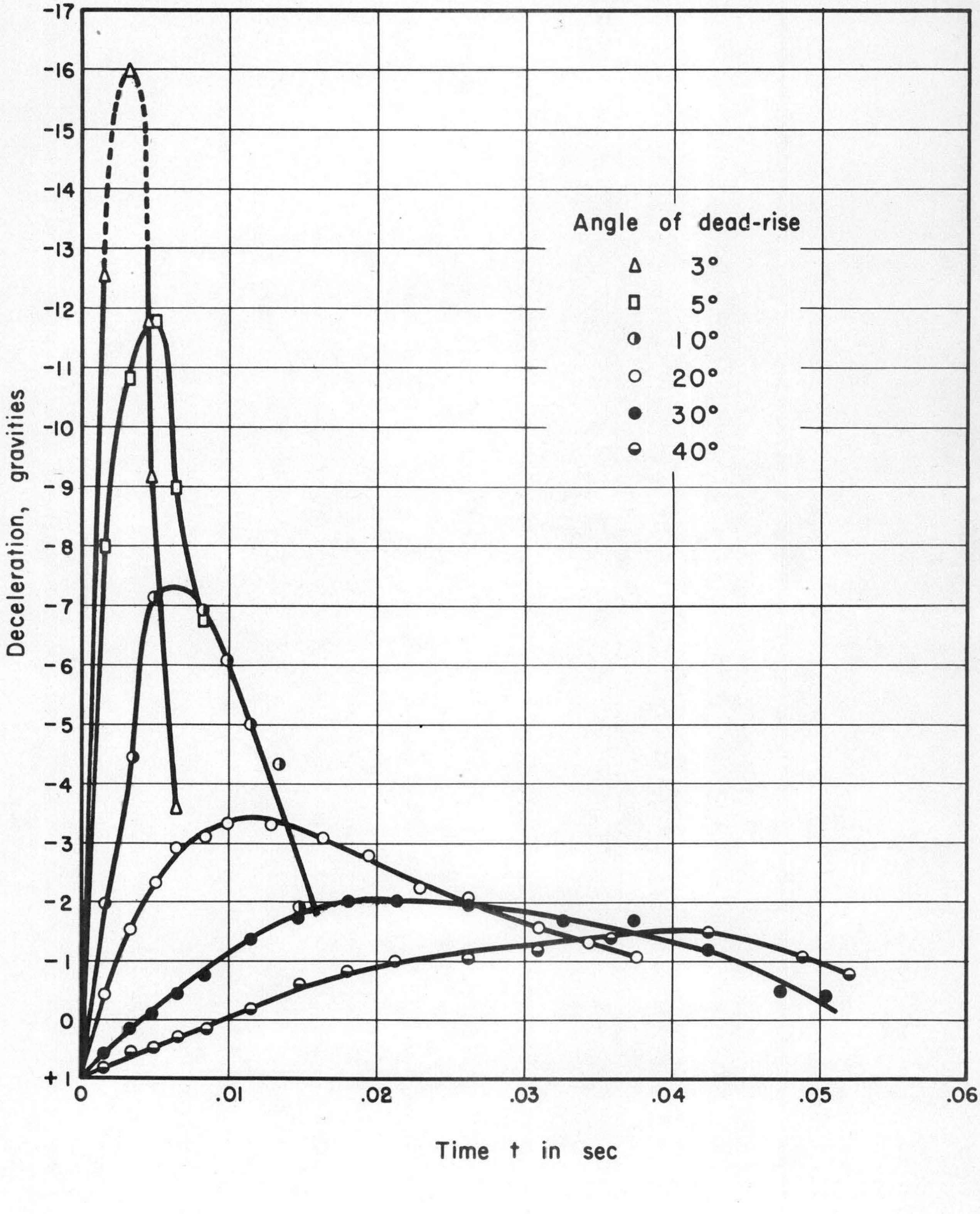

Fig. 6 Variation of the deceleration with time for V-wedges

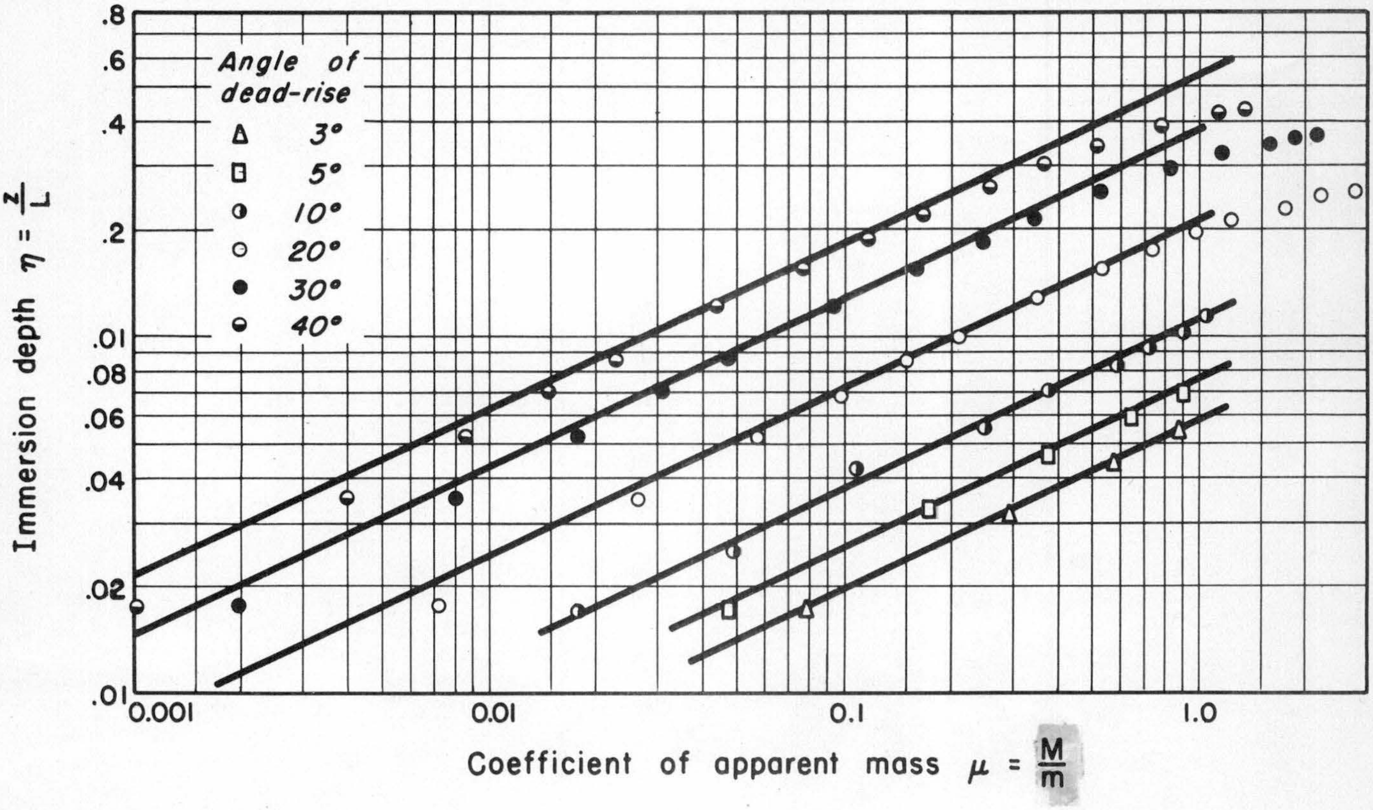

Fig. 7 Variation of coefficient of apparent mass μ with respect to immersion depth η for V-wedges

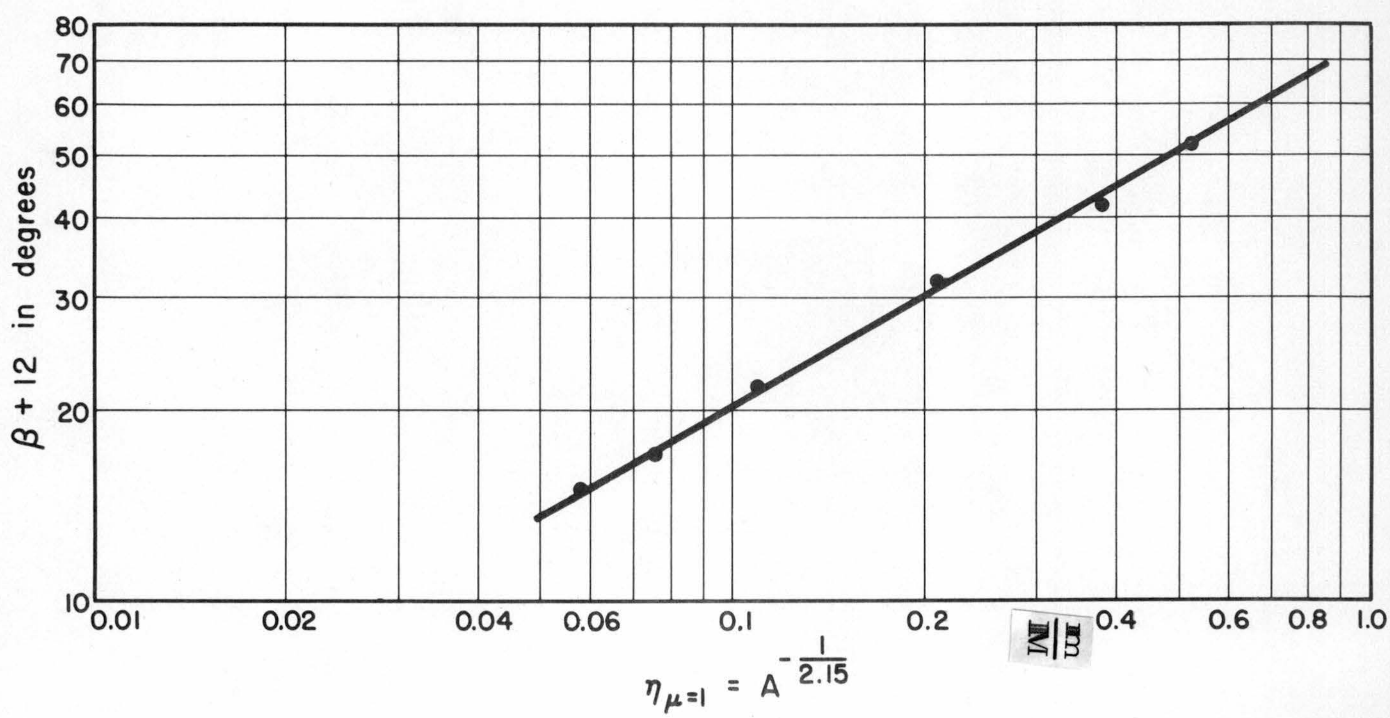

Fig. 8 Variation of the immersion depth η at $\mu = 1$ with angle of dead-rise β for V-wedges

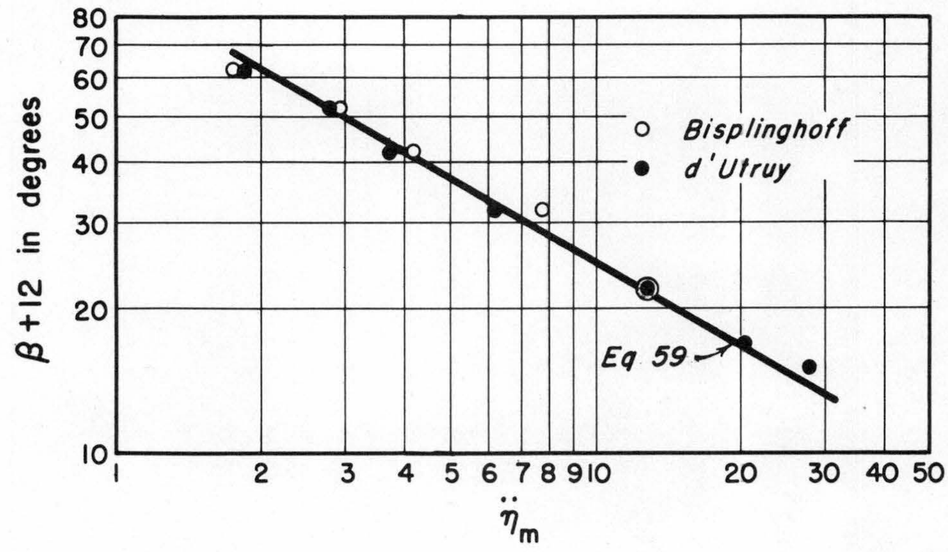

Fig. 9 Variation of maximum deceleration $\ddot{\eta}_m$ with angle of dead-rise β for V-wedges

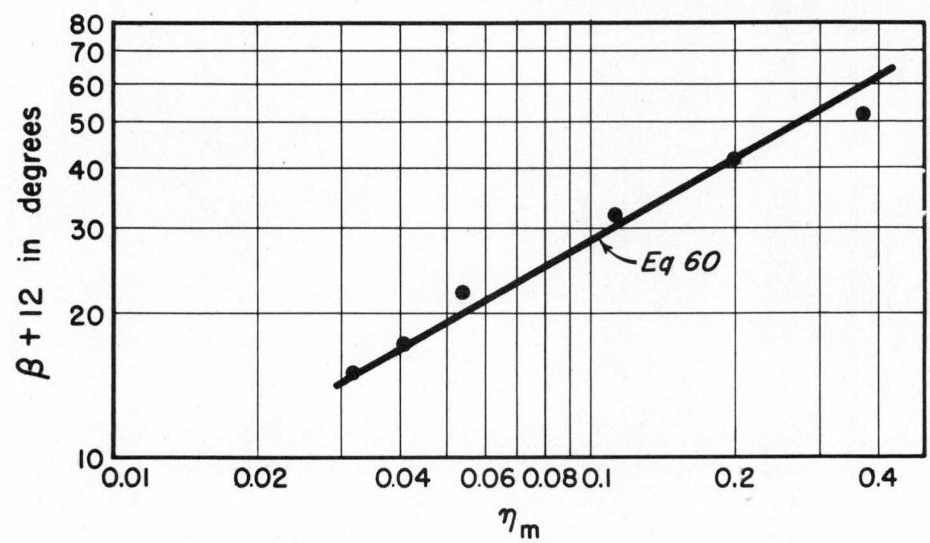

Fig. 10 Variation of immersion depth η_m to maximum deceleration $\ddot{\eta}_m$ with angle of dead-rise β for V-wedges

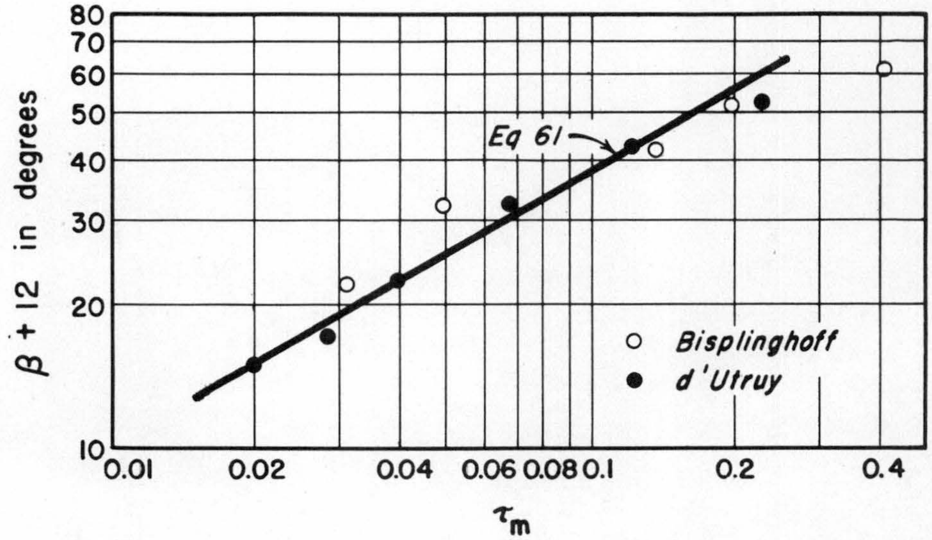

Fig. 11 Variation of time τ_m to maximum deceleration η_m with angle of dead-rise β for V-wedges

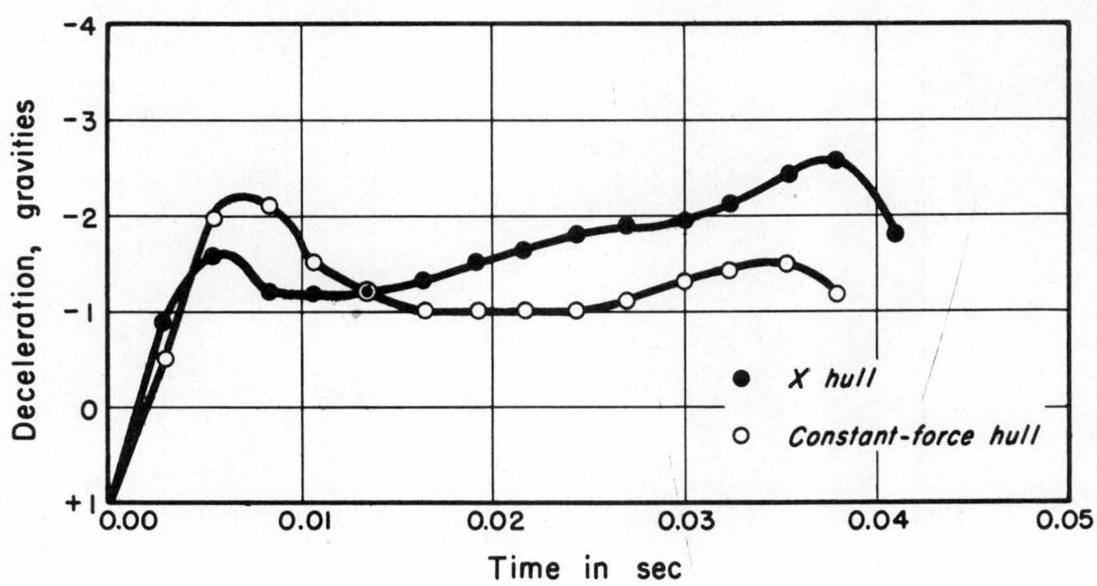

Fig. 12 Variation of the deceleration with time for constant - force hulls

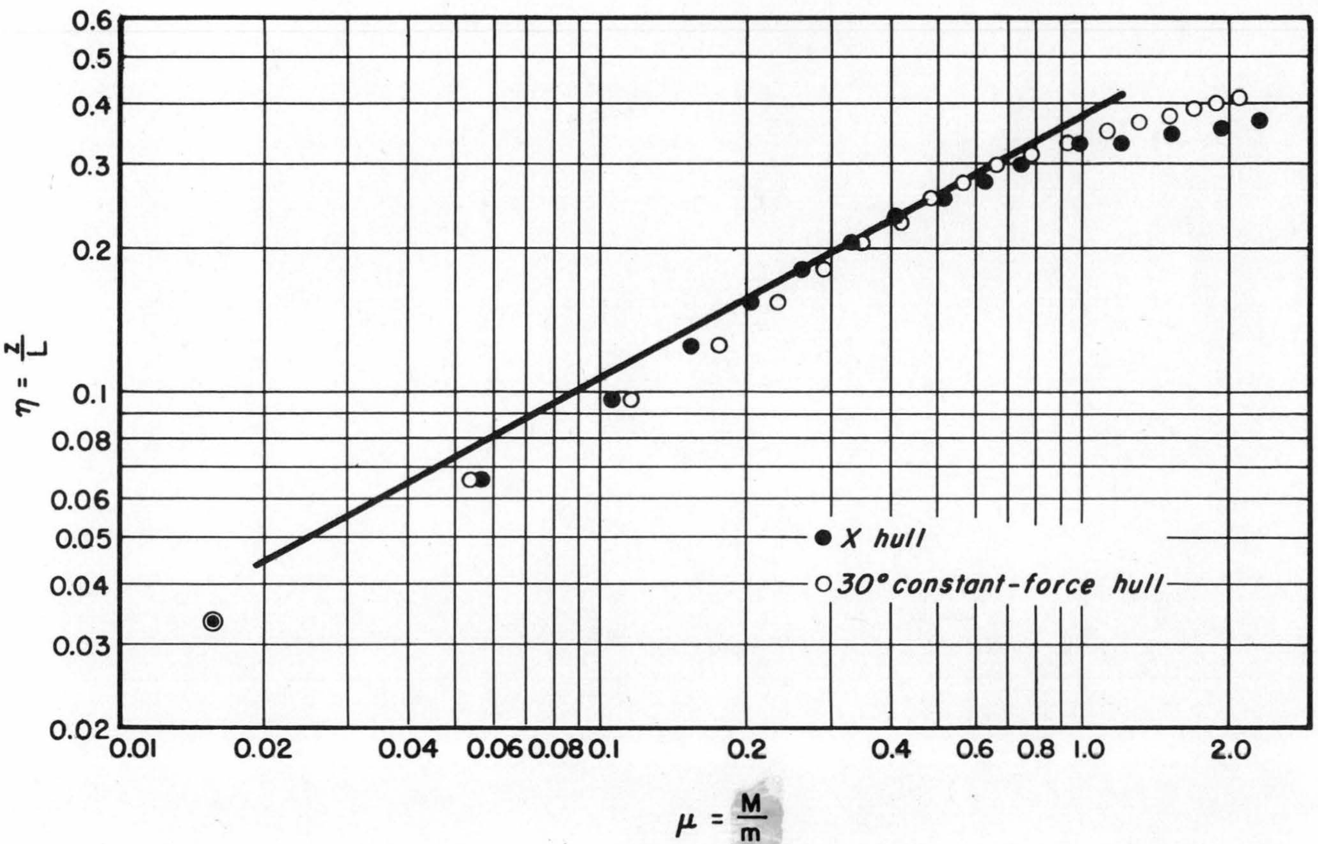

Fig. 13 Variation of coefficient of apparent mass μ with immersion depth η for constant-force hulls

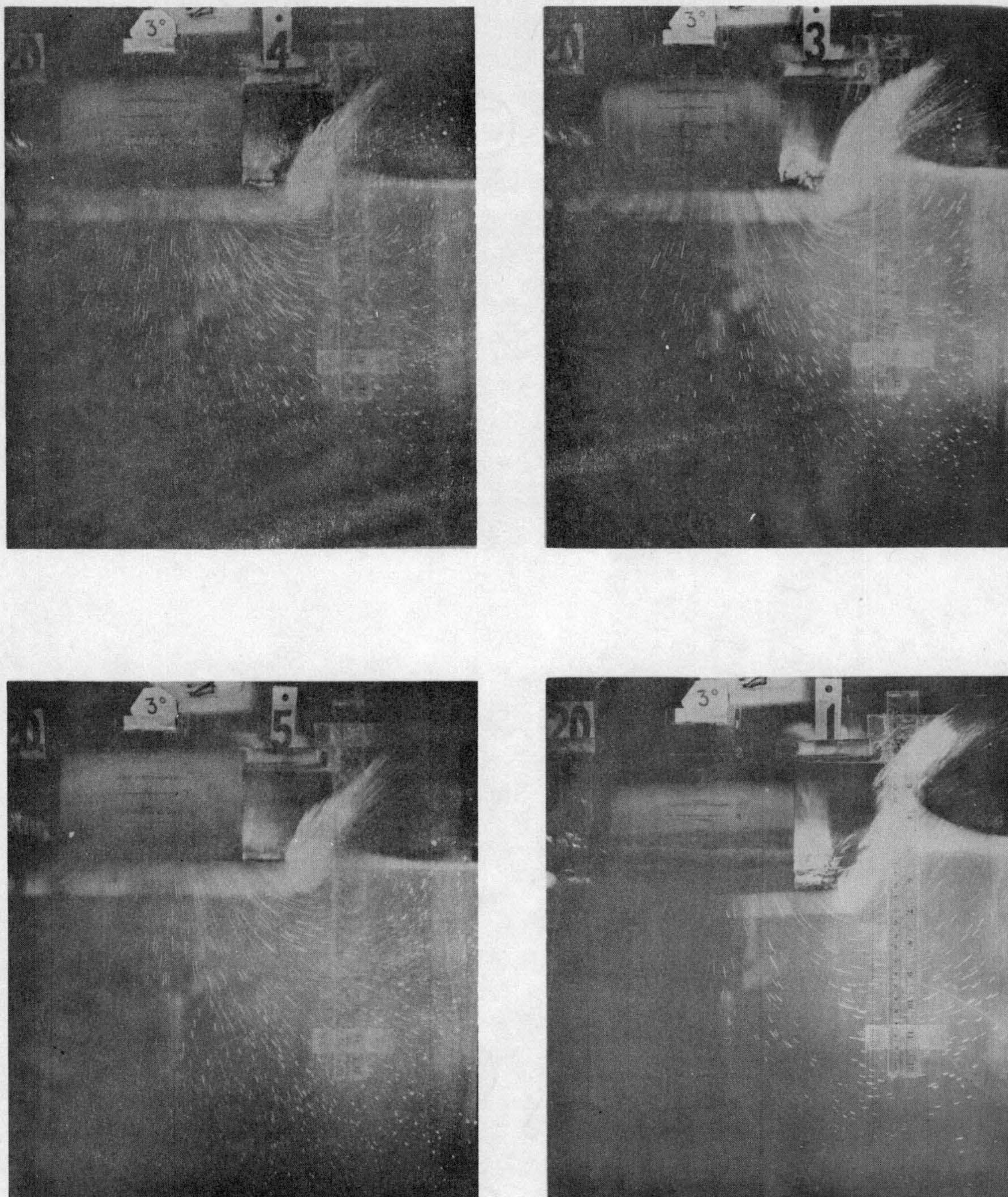

Fig.14 3° Wedge, flow field at several immersion depths during impact

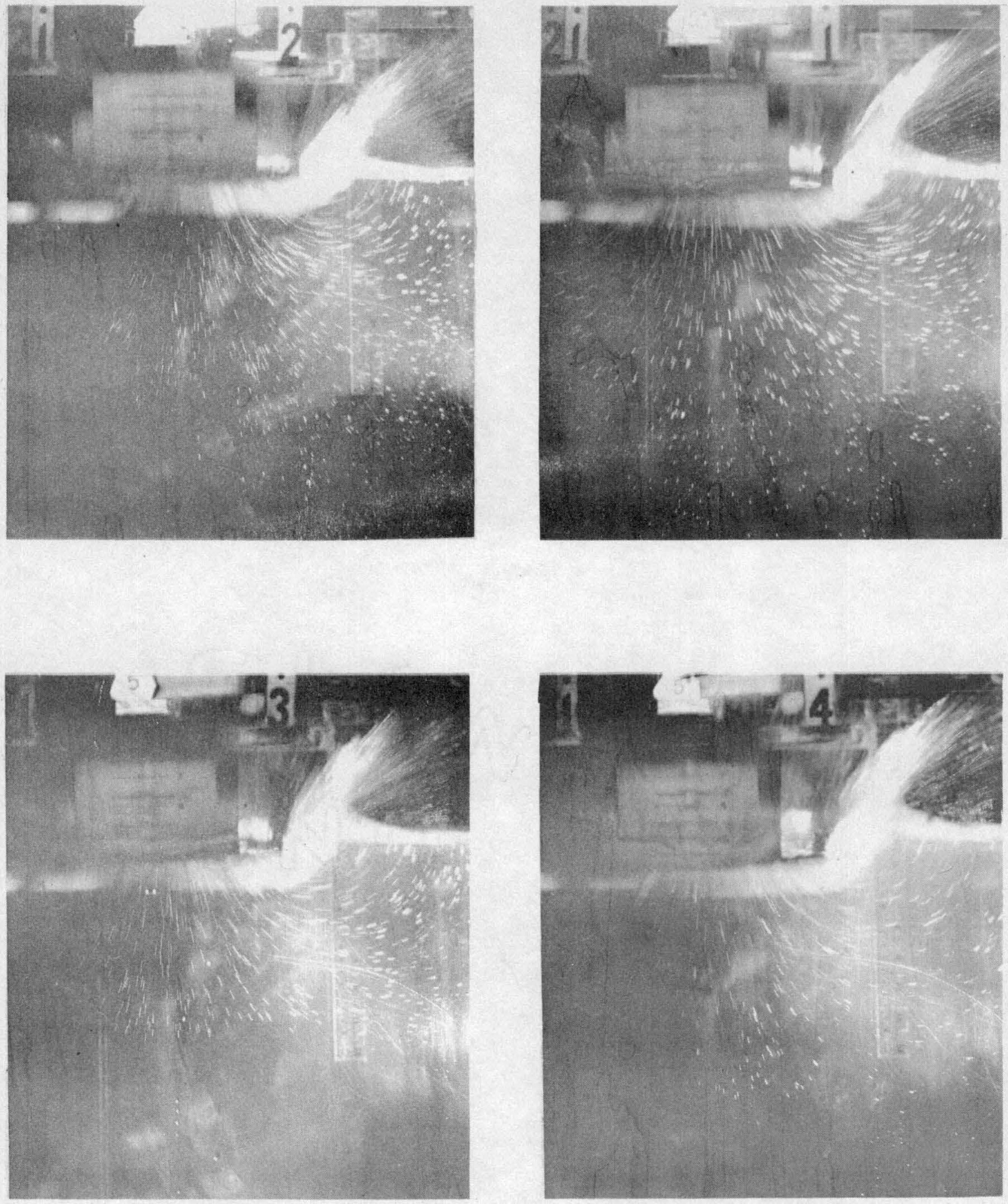

Fig. 15 5^{o} Wedge, flow field at several immersion depths during impact

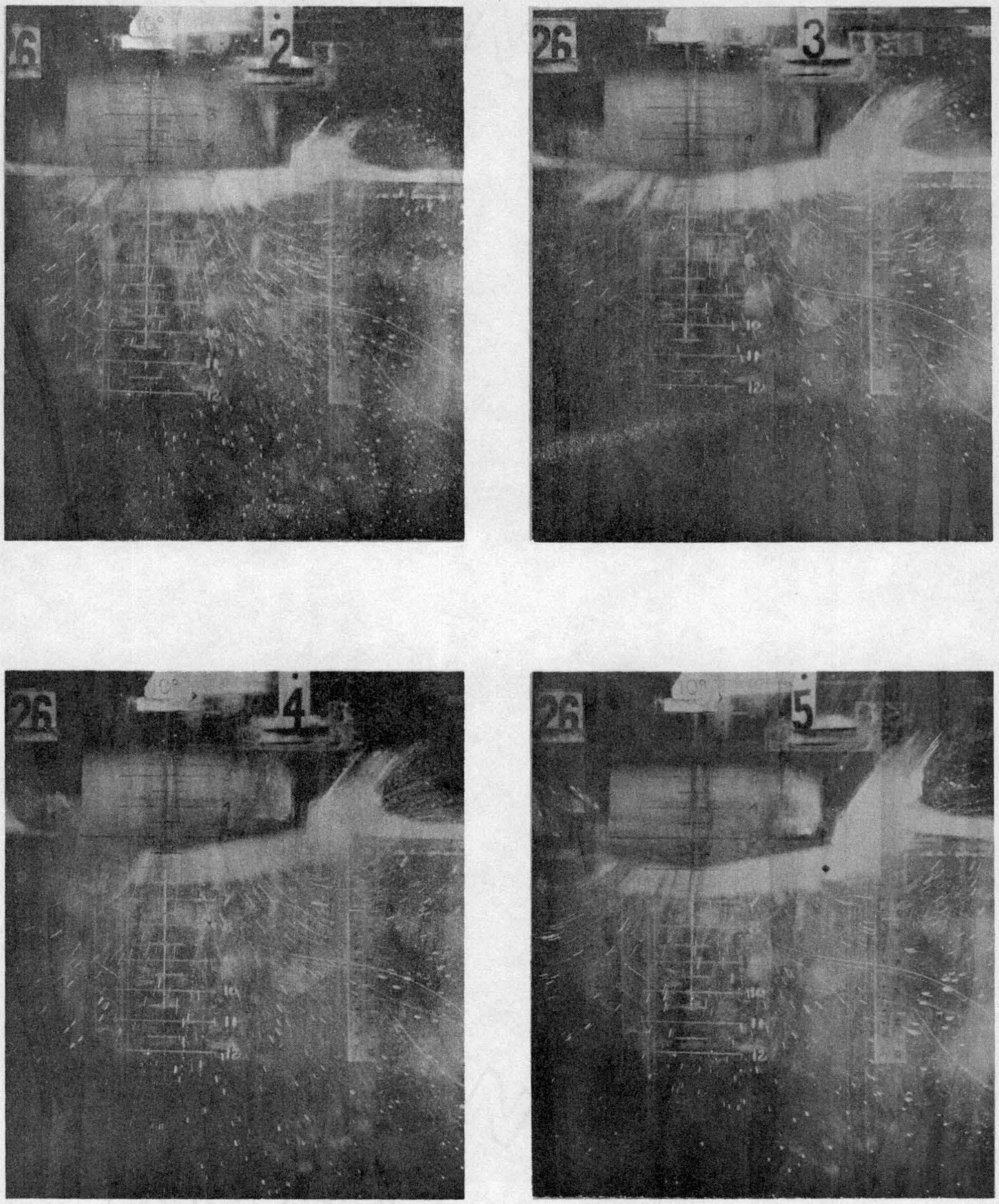

Fig.16 10° Wedge, flow field at several immersion depths during impact

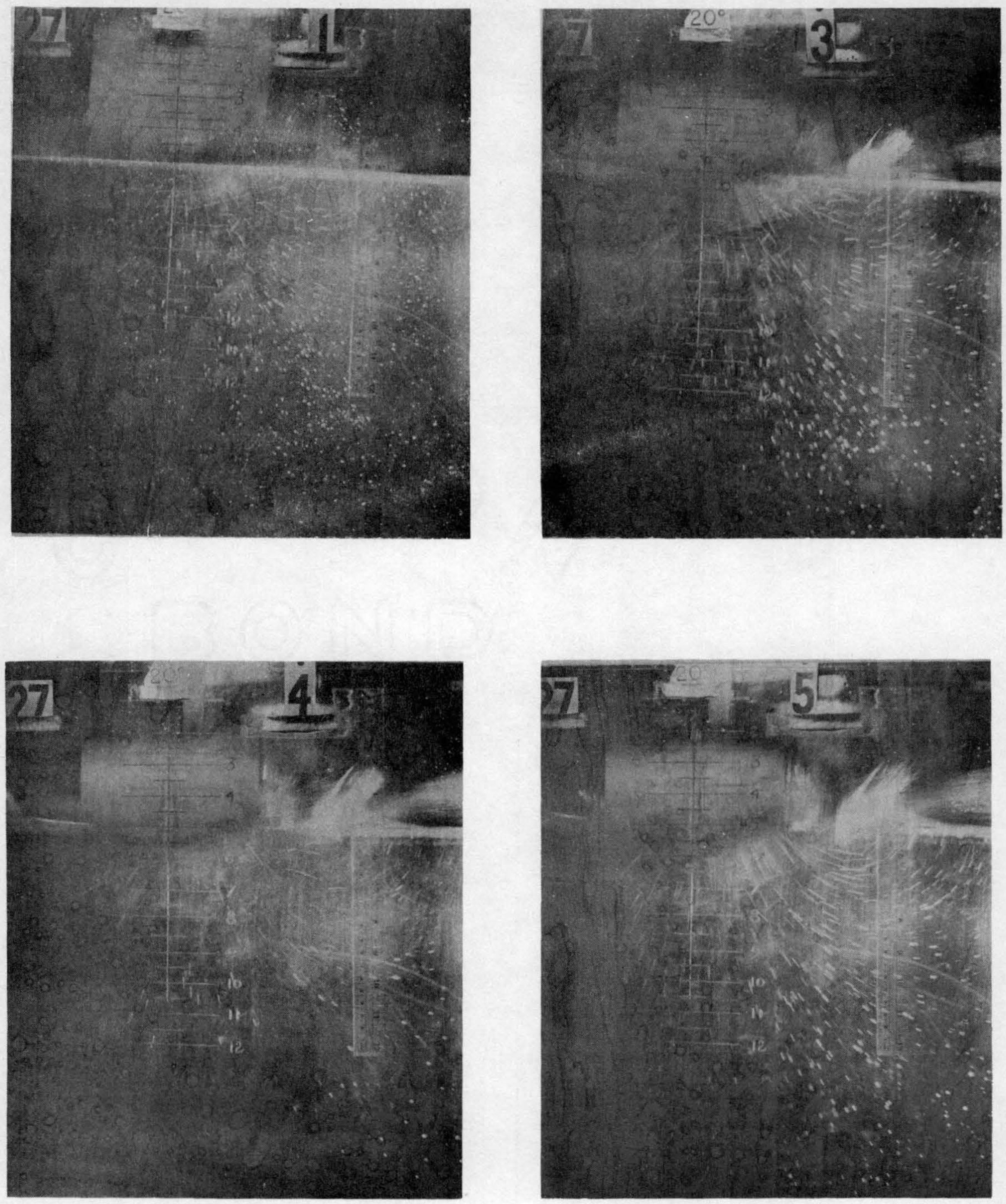

Fig. 17 20° Wedge, flow field at several immersion depths during impact.

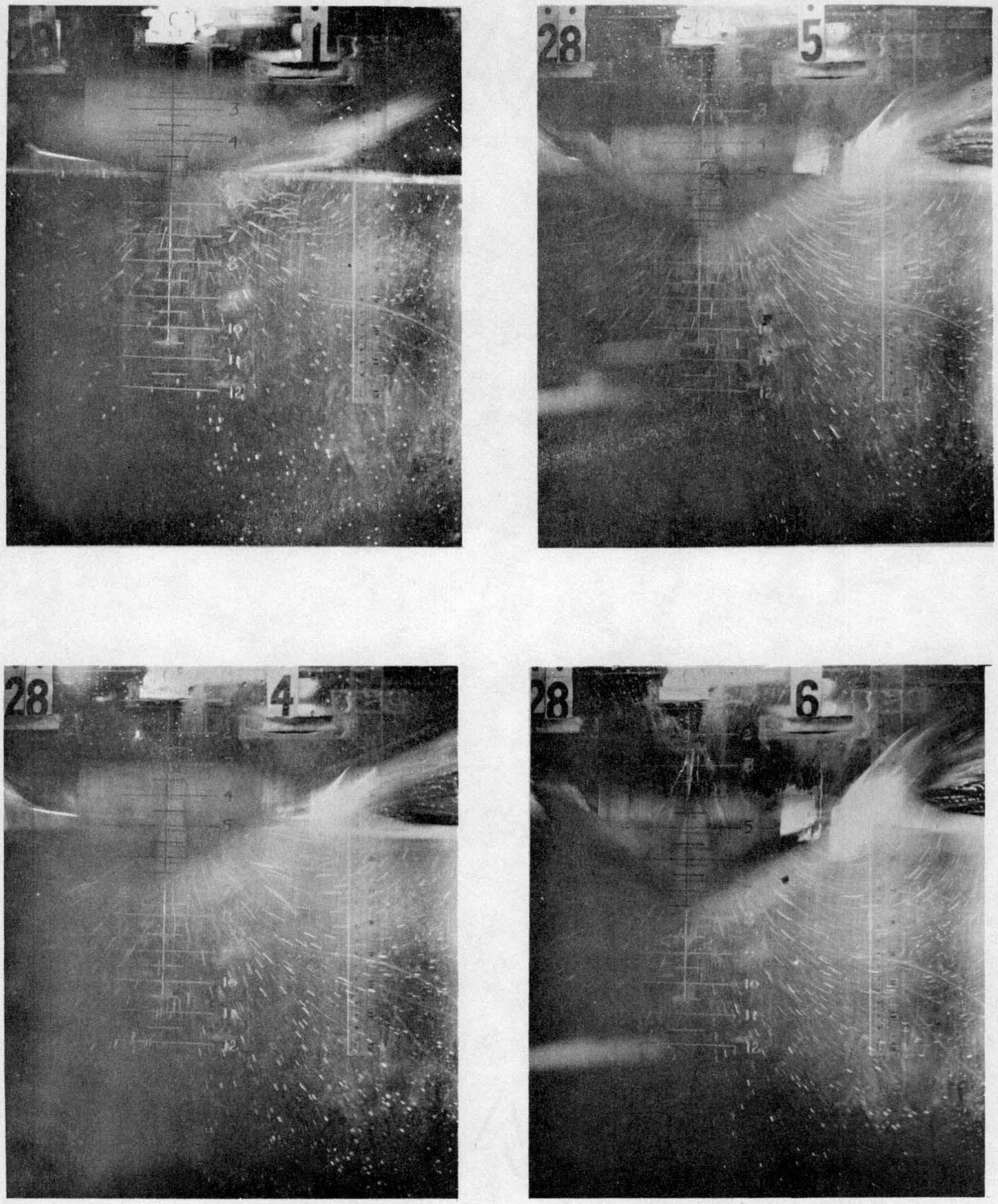

Fig.18 30° Wedge, flow field at several immersion depths during impact

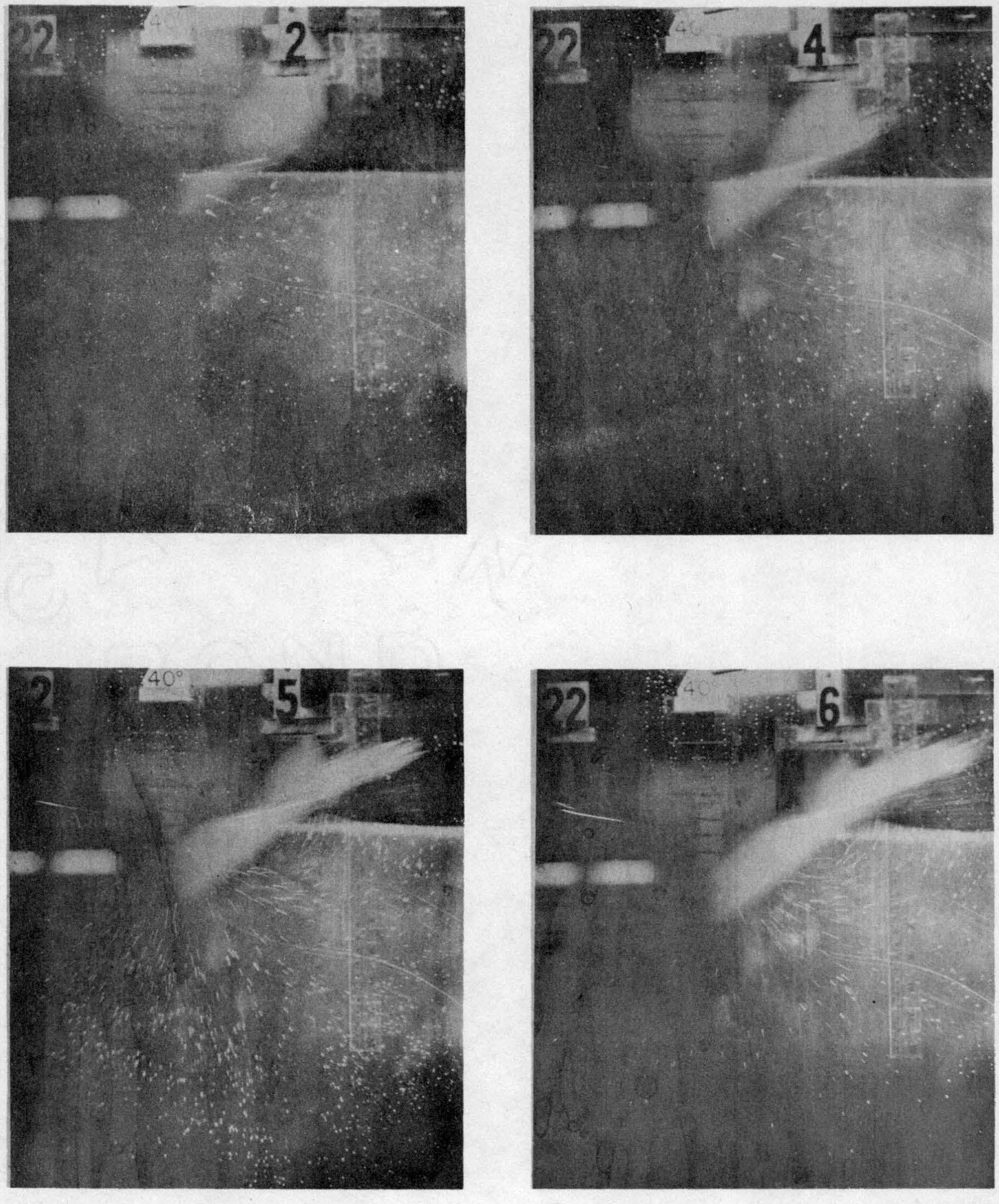

Fig. 19 40° Wedge, flow field at several immersion depths during impact

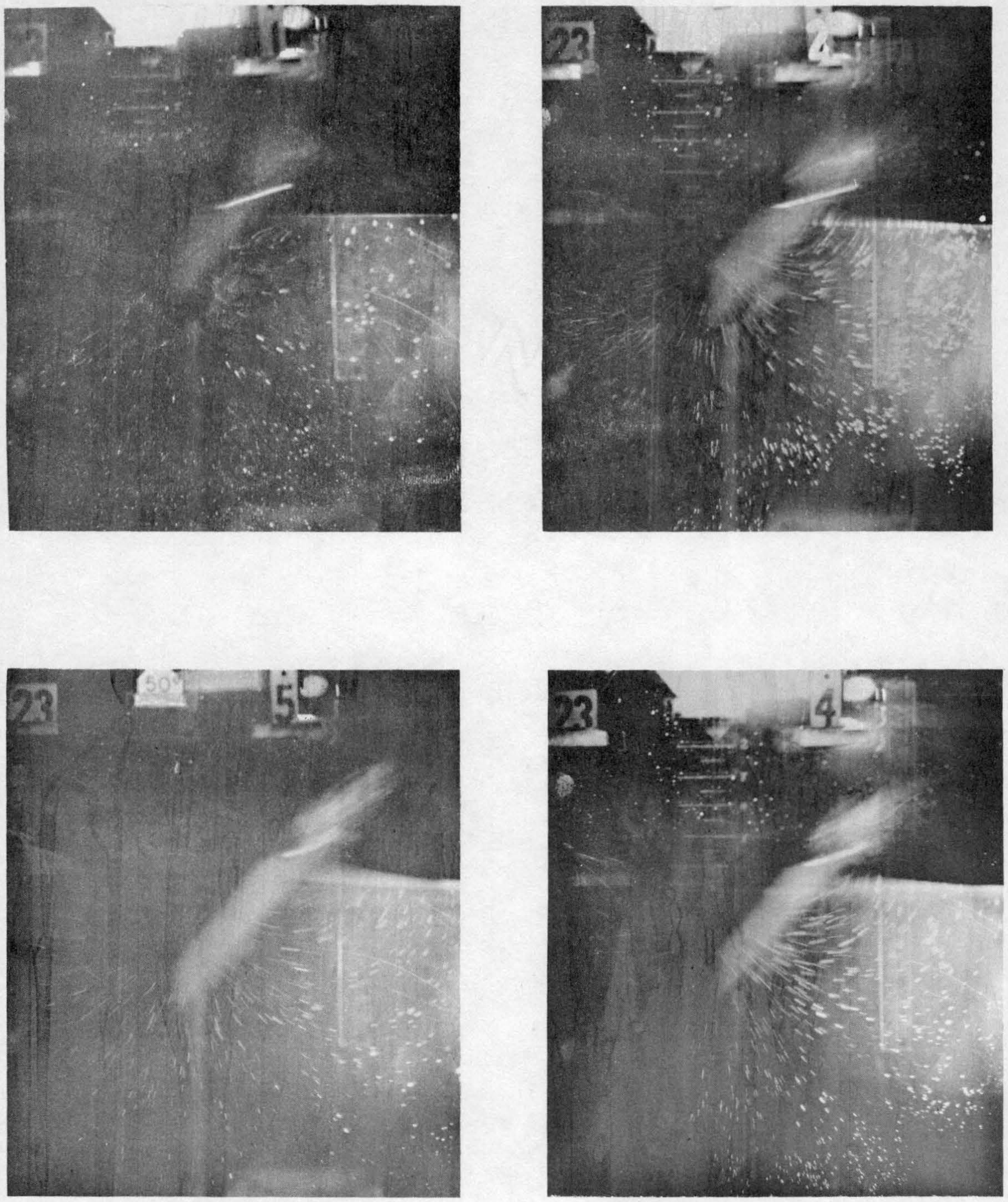

Fig. 20 50° Wedge, flow field at several immersion depths during impact

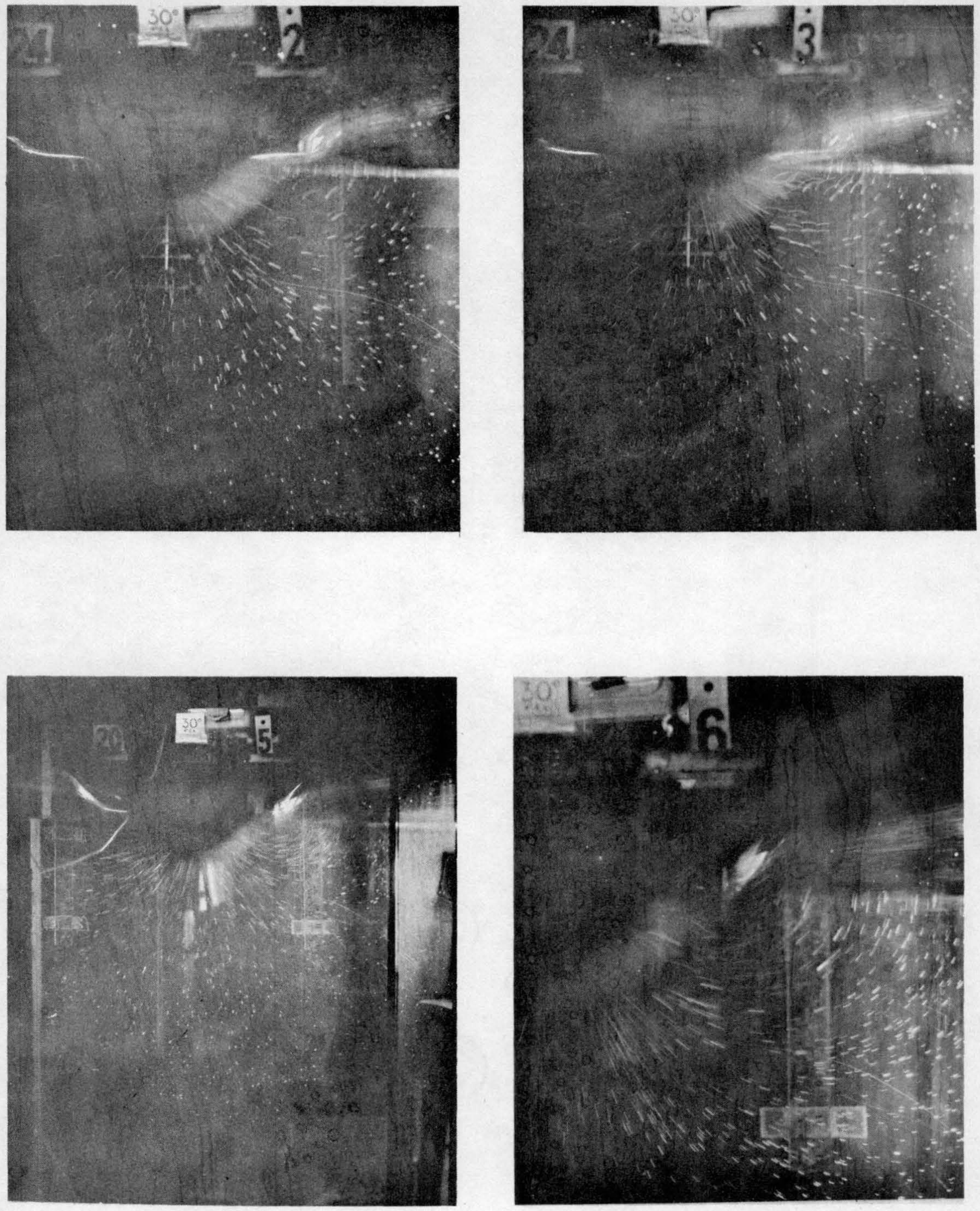

Fig. 21 30° CTE Force Hull

Flow field at several immersion depths during impact

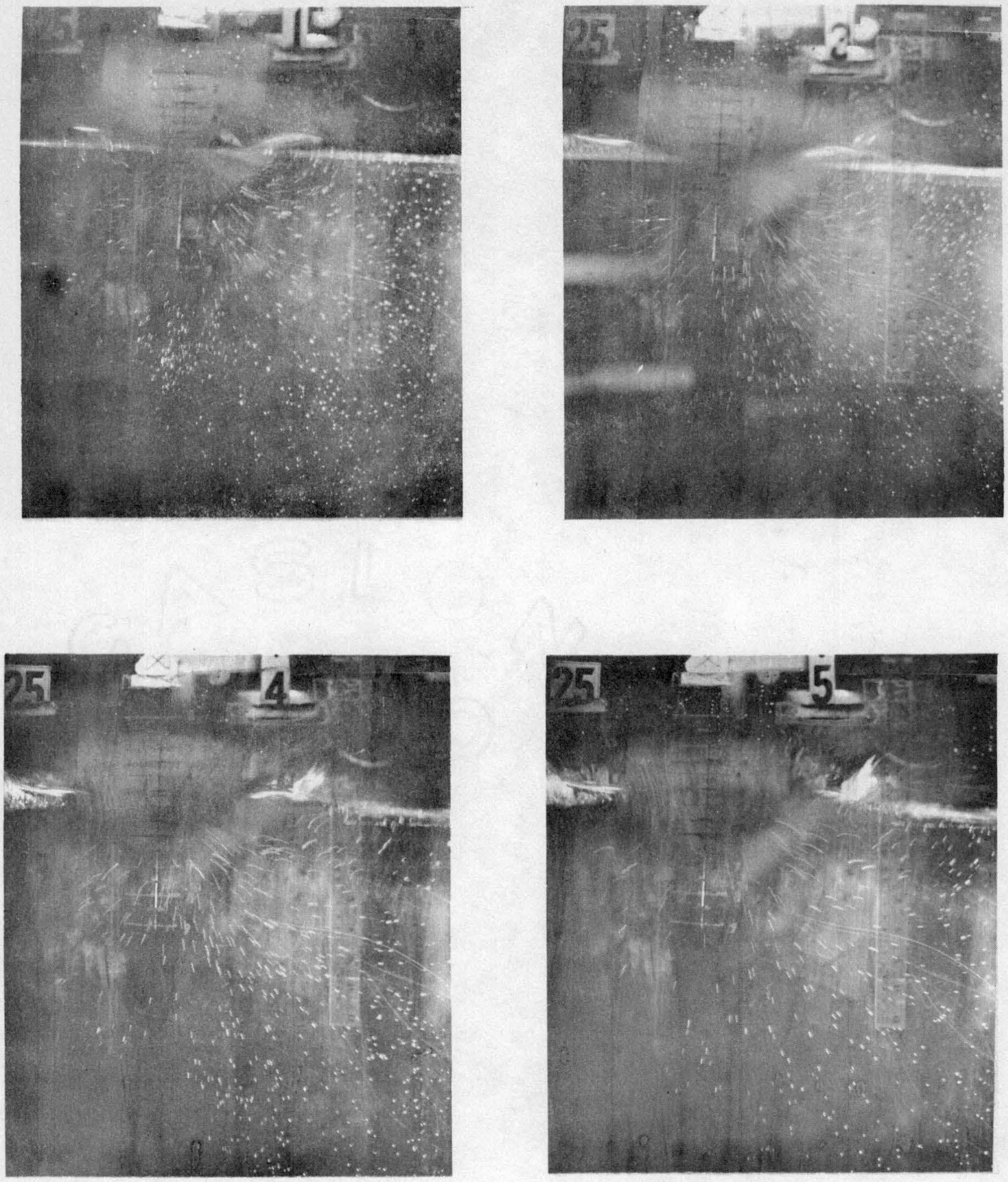

Fig.22 X-Hull

Flow field at several immersion depths during impact

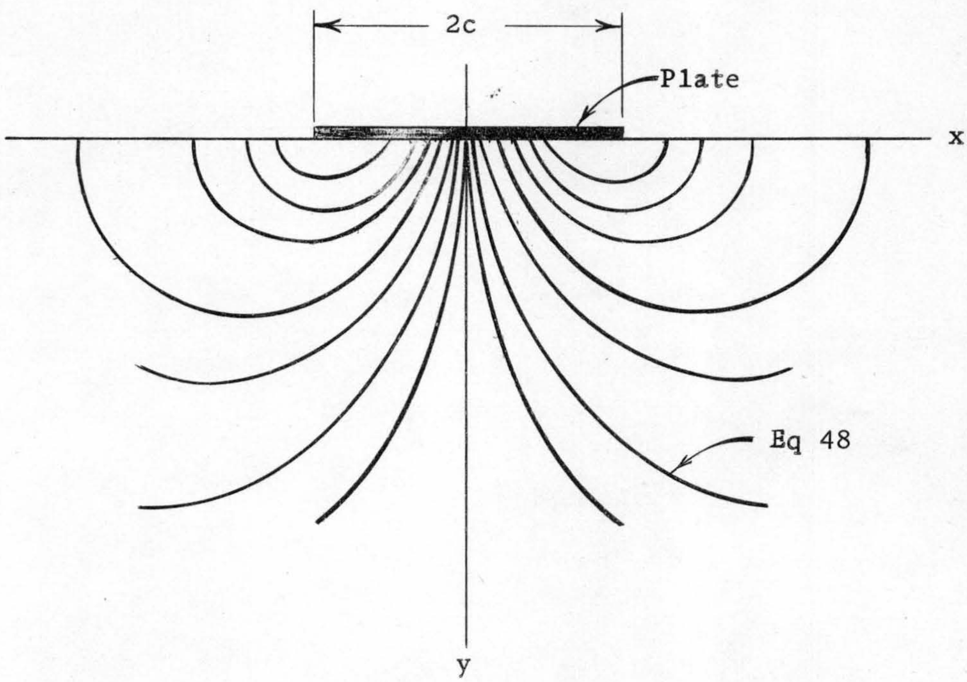

Fig. 23 Flow field around a plate, unsteady case

A P P E N D I X

TABLE OF CONTENTS

APPENDIX A

GEOMETRIC DIMENSIONS OF V-WEDGE HULLS

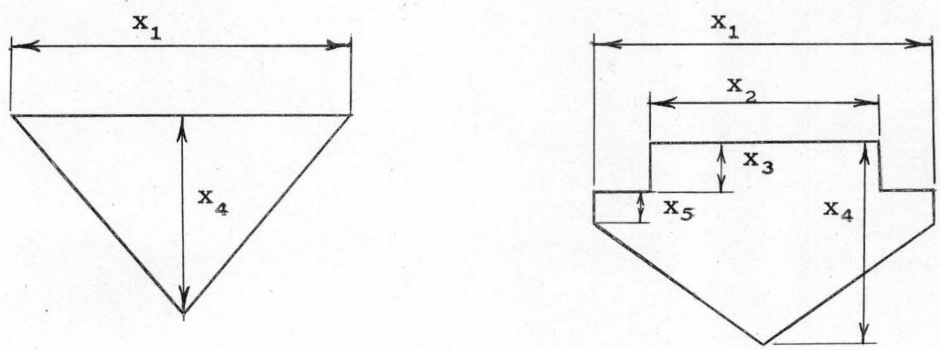

Cross-section of V-wedge hulls

β	3°	5°	10°	20°	30°	40°	50°
X_1	9.35	9.35	9.50	9.50	9.50	9.50	9.50
X_2	6.35	6.40	6.00	6.10	6.30	0	0
X_3	2.95	2.70	1.50	1.90	0.50	0	0
X_4	3.75	3.75	3.50	3.85	3.75	4.00	7.60
X_5	0.35	0.60	1.20	0.35	0.35	0	0

All dimensions of hulls are expressed in inches

APPENDIX B

GEOMETRIC DIMENSIONS OF X-HULL

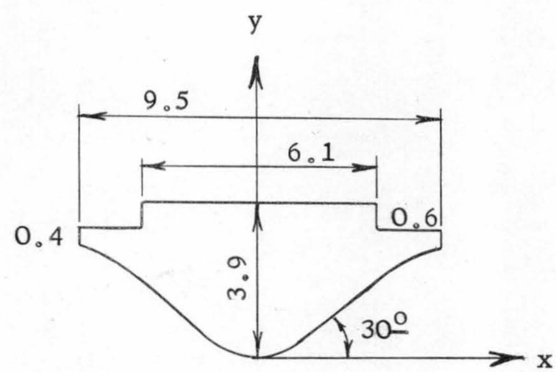

Cross-section of X-hull tested

x*	0.579	1.158	1.737	2.316	2.895	3.474	4.053	4.632	5.211	5.500
y*	0.08	0.36	0.83	1.33	1.84	2.36	2.87	3.22	3.34	3.32
X	0.50	1.00	1.50	2.00	2.50	3.00	3.50	4.00	4.50	4.75
Y	0.066	0.297	0.685	1.099	1.520	1.947	2.360	2.660	2.760	2.740

Coordinates in inches (XY) of contour of X-hull expressed in inches

APPENDIX C

GEOMETRIC DIMENSIONS OF 30° CONSTANT FORCE HULL

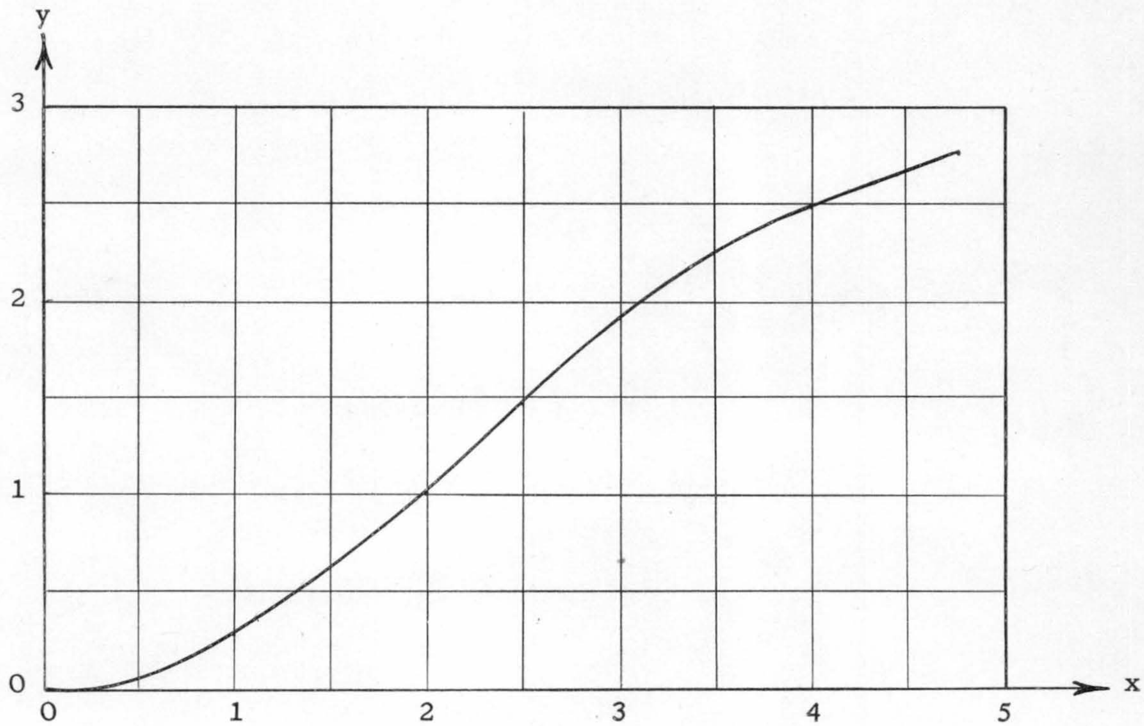

Coordinates in inches of 30° constant-force hull expressed in inches

APPENDIX D

SUMMARY OF COMPUTED QUANTITIES

3 degree V-wedge

t sec	a_n gravities		V_n fps	μ_n	η_n
0.0000	0.0		5.18	0.000	0.0000
0.0016	13.6		4.82	0.075	0.0173
0.0033	17	(estimated)	4.01	0.29	0.0325
0.0049	10.2		3.30	0.57	0.0450
0.0065	4.5		2.91	0.78	0.0560

$\ddot{\eta}_m$ = 28 (estimated)

t_m = 0.033 sec (estimated)

η_m = 0.032 (estimated)

5 degree V-wedge

t sec	a_n gravities	V_n fps	μ_n	η_n
0.0000	0.0	0.00	0.0000	0.0000
0.0016	9.0	5.18	0.0475	0.0174
0.0033	11.8	4.94	0.172	0.0335
0.0049	12.8	4.42	0.372	0.0476
0.0065	10.0	3.78	0.631	0.0596
0.0083	7.8	3.18	0.911	0.0697

$\ddot{\eta}_m$ = 20.7

t_m = 0.0045

η_m = 0.041

10 degree V-wedge

t_n sec	a_n gravities	V_n fps	μ_n	η_n
0.0000	0.0	5.18	0.000	0.0000
0.0016	2.9	5.10	0.015	0.0177
0.0033	5.4	4.94	0.050	0.0250
0.0049	8.2	4.58	0.108	0.0414
0.0065	8.1	4.15	0.250	0.0564
0.0083	7.8	3.74	0.387	0.0700
0.0098	7.1	3.35	0.595	0.0822
0.0114	6.0	3.01	0.720	0.0932
0.0131	5.3	2.71	0.910	0.103
0.0147	2.8	2.51	1.064	0.112

$\ddot{\eta}_m = 12.7$

$t_m = 0.0064$ sec

$\eta_m = 0.054$

20 degree V-wedge

t_n sec	a_n gravities	V_n fps	μ_n	η_n
0.0000	0.0	5.18	0.00000	0.0000
0.0016	1.4	5.14	0.00719	0.0177
0.0033	2.5	5.05	0.0266	0.0353
0.0049	3.3	4.90	0.0573	0.0524
0.0065	3.9	4.71	0.0998	0.0689
0.0083	4.1	4.50	0.151	0.0847
0.0098	4.3	4.28	0.210	0.0998
0.0131	4.3	3.83	0.352	0.128
0.0163	4.1	3.39	0.528	0.153
0.0196	3.6	2.98	0.736	0.175
0.0229	3.2	2.63	0.972	0.194
0.0261	3.1	2.30	1.253	0.211
0.0310	2.6	1.84	1.807	0.232
0.0343	2.3	1.59	2.256	0.244
0.0376	2.1	1.36	2.809	0.254

$\ddot{\eta}_m = 6.1$

$t_m = 0.011$ sec

$\eta_m = 0.11$

30 degree V-wedge

t_n sec	a_n gravities	V_n fps	μ_n	η_n
0.0000	0.0	5.18	0.00000	0.0000
0.0016	0.4	5.17	0.00197	0.0178
0.0033	0.8	5.14	0.00811	0.0356
0.0049	1.1	5.09	0.0180	0.0533
0.0065	1.4	5.02	0.0312	0.0709
0.0083	1.7	4.94	0.0474	0.0883
0.0114	2.4	4.73	0.0944	0.122
0.0147	2.7	4.46	0.160	0.155
0.0180	3.0	4.16	0.244	0.185
0.0212	3.0	3.85	0.346	0.214
0.0261	2.9	3.38	0.533	0.253
0.0327	2.7	2.80	0.852	0.297
0.0376	2.7	2.37	1.189	0.326
0.0425	2.2	1.97	1.622	0.348
0.0474	1.5	1.77	1.921	0.362
0.0506	1.4	1.61	2.211	0.374

$\ddot{\eta}_m = 3.7$

$t_m = 0.020$ sec

$\eta_m = 0.20$

40 degree V-wedge

t_n sec	a_n gravities	V_n fps	μ_n	η_n
0.0000	0.0	5.18	0.00000	0.0000
0.0016	0.2	5.17	0.00101	0.0178
0.0033	0.4	5.16	0.00404	0.0356
0.0049	0.5	5.13	0.00865	0.0533
0.0065	0.7	5.10	0.0149	0.0709
0.0083	0.8	5.06	0.0228	0.0884
0.0114	1.2	4.96	0.0445	0.123
0.0147	1.6	4.81	0.0764	0.156
0.0180	1.8	4.63	0.118	0.188
0.0212	2.0	4.43	0.168	0.220
0.0261	2.1	4.11	0.259	0.264
0.0310	2.2	3.78	0.372	0.305
0.0359	2.4	3.41	0.519	0.342
0.0425	2.4	2.89	0.792	0.385
0.0490	2.1	2.41	1.149	0.422
0.0523	1.8	2.20	1.351	0.438

$\ddot{\eta}_m = 2.7$

$t_m = .040$ sec

$\eta_m = 0.37$

30 degree constant-force hull

t_n sec	a_n gravities	V_n fps	μ_n	η_n
0.00000	0.0	5.18	0.0000	0.0000
0.00273	1.5	5.11	0.0157	0.0333
0.00545	3.0	4.91	0.0540	0.0657
0.00818	3.1	4.64	0.116	0.0966
0.0109	2.5	4.40	0.177	0.126
0.0136	2.2	4.20	0.233	0.154
0.0163	2.0	4.01	0.291	0.180
0.0191	2.0	3.83	0.352	0.206
0.0218	2.0	3.65	0.419	0.230
0.0245	2.0	3.48	0.488	0.253
0.0273	2.1	3.29	0.574	0.275
0.0800	2.3	3.10	0.670	0.295
0.0327	2.4	2.89	0.792	0.315
0.0354	2.5	2.67	0.940	0.333
0.0381	2.2	2.43	1.132	0.349

$\ddot{\eta}_m = 3.7$

$t_m = 0.0080$ sec

$\eta_m = 0.12$

X-hull

t_n sec	a_n gravities	V_n fps	μ_n	η_n
0.00000	0.0	5.18	0.0000	0.0000
0.00273	1.9	5.10	0.0157	0.0333
0.00545	2.6	4.90	0.057	0.0656
0.00818	2.2	4.68	0.107	0.0966
0.0109	2.2	4.49	0.154	0.126
0.0136	2.8	4.29	0.207	0.155
0.0163	2.3	4.09	0.266	0.182
0.0191	2.5	3.88	0.335	0.208
0.0218	2.6	3.66	0.415	0.232
0.0245	2.8	3.42	0.514	0.255
0.0273	2.9	3.16	0.639	0.276
0.0300	3.0	2.90	0.750	0.296
0.0327	3.1	2.63	0.969	0.314
0.0354	3.4	2.34	1.213	0.330
0.0381	3.6	2.03	1.551	0.344

$\ddot{\eta}_m = 4.5$

$t_m = 0.038$ sec

$\eta_m = 0.34$